THE "YEAR" OF TROPICAL CONVECTION (MAY 2008–APRIL 2010)

Climate Variability and Weather Highlights

BY DUANE E. WALISER, MITCHELL W. MONCRIEFF, DAVID BURRIDGE, ANDREAS H. FINK, DAVE GOCHIS, B. N. GOSWAMI, BIN GUAN, PATRICK HARR, JULIAN HEMING, HUANG-HSUING HSU, CHRISTIAN JAKOB, MATT JANIGA, RICHARD JOHNSON, SARAH JONES, PETER KNIPPERTZ, JOSE MARENGO, HANH NGUYEN, MICK POPE, YOLANDE SERRA, CHRIS THORNCROFT, MATTHEW WHEELER, ROBERT WOOD, AND SANDRA YUTER

May 2008–April 2010 provided a diverse array of scientifically interesting and socially important weather and climate events that emphasizes the impact and reach of tropical convection over the globe.

The realistic representation of tropical convection in our global atmospheric models is a long-standing grand challenge for numerical weather forecasts and global climate predictions [see companion article Moncrieff et al. (2012), hereafter M12]. Our lack of fundamental knowledge and practical capabilities in this area leaves us disadvantaged in simulating and/or predicting prominent phenomena of the tropical atmosphere, such as the intertropical convergence zone (ITCZ), El Niño–Southern Oscillation (ENSO), monsoons and their active/break periods, the Madden–Julian oscillation (MJO), easterly waves and tropical cyclones, subtropical stratus decks, and even the diurnal cycle. Furthermore, tropical climate and weather disturbances strongly influence stratospheric–tropospheric exchange and the extratropics. To address this challenge, the World Climate Research Programme (WCRP) and The Observing System Research and Predictability Experiment (THORPEX) of the World Weather

AFFILIATIONS: WALISER AND GUAN—Jet Propulsion Laboratory, California Institute of Technology, Pasadena, California; MONCRIEFF, GOCHIS, AND GOSWAMI—National Center for Atmospheric Research, Boulder, Colorado; BURRIDGE—THORPEX, World Meteorological Organization, Geneva, Switzerland; FINK—Institute of Geophysics and Meteorology, University of Cologne, Cologne, Germany; GOSWAMI—Indian Institute of Tropical Meteorology, Pune, India; HARR—Naval Postgraduate School, Monterey, California; HEMING—Met Office, Exeter, United Kingdom; HSU—National Taiwan University, Taipei, Taiwan; JAKOB—Monash University, Melbourne, Victoria, Australia; JANIGA, NGUYEN, AND THORNCROFT—University at Albany, State University of New York, Albany, New York; JOHNSON—Colorado State University, Fort Collins, Colorado; JONES—Karlsruhe Institute of Technology, Karlsruhe, Germany; KNIPPERTZ—University of Leeds, Leeds, United Kingdom; MARENGO—Centro de Previsão de Tempo e Estudos Climáticos, Sao Paulo, Brazil; POPE—Bureau of Meteorology Training Centre, Bureau of Meteorology, Melbourne, Victoria, Australia; SERRA—University of Arizona, Tucson, Arizona; WHEELER—Centre for Australian Weather and Climate Research, Melbourne, Victoria, Australia; WOOD—University of Washington, Seattle, Washington; YUTER—North Carolina State University, Raleigh, North Carolina
CORRESPONDING AUTHOR: Duane Waliser, Jet Propulsion Laboratory, MS 183–505, California Institute of Technology, 4800 Oak Grove Drive, Pasadena, CA 91109
E-mail: duane.waliser@jpl.nasa.gov

The abstract for this article can be found in this issue, following the table of contents.
DOI:10.1175/2011BAMS3095.1

In final form 1 August 2011

Research Programme (WWRP) jointly proposed and are implementing a coordinated research program involving observing, modeling, and forecasting of organized tropical convection—referred to as the "Year of Tropical Convection" (see www.ucar.edu/yotc). A key component of the motivation of YOTC is that there have been substantial investments in Earth science infrastructure over the previous decades. These are now realized in terms of a comprehensive satellite-observing system (e.g., Earth Observing System), operational buoy arrays in each of the tropical oceans, global analyses and forecast systems that are now carried out at resolutions less than 25 km, and a number of global, high-resolution, convection-permitting modeling systems. Based on these investments, including field programs already in place, a key precept of YOTC is that a tractable and promising research program can be constructed from the presently available resources, through a focus period approach, in much the same way field programs and specific phenomenological cases focus and magnify the community's attention and efforts [e.g., the First Global Atmospheric Research Program (GARP) Global Experiment (FGGE), and the Tropical Ocean and Global Atmosphere Coupled Ocean–Atmosphere Response Experiment (TOGA COARE)].

The YOTC period is from May 2008 to April 2010; its choice developed from deliberations that started with the activity's conception at a WCRP–THORPEX-sponsored meeting in 2006 (Moncrieff et al. 2007), its subsequent science planning meeting in 2007 (Waliser and Moncrieff 2008), and the YOTC implementation planning meeting in 2009 (see the implementation plan at www.ucar.edu/yotc). While the target period was initially designed to be a year, its extension to a full 2 yr was proposed and agreed to at the implementation planning meeting in concert with the realization that a second year would allow YOTC to capture a period of both La Niña and El Niño conditions (see Fig. 1). In this article, we describe this period in terms of its anomalous low-frequency characteristics as well as highlight the most interesting and impactful synoptic features. The description of the latter is largely aligned with the targeted phenomenological areas outlined in the YOTC Science Plan. These include 1) the MJO and other convectively coupled equatorial waves (CCEWs), 2) easterly waves and tropical cyclones (TCs), 3) monsoons, 4) tropical–extratropical interactions, and 5) the diurnal cycle. The objective of this overview article is to set the stage for more targeted and in-depth observation, modeling, and prediction studies for the YOTC period, following the strategies outlined in the YOTC Implementation Plan. Following the descriptions of the low-frequency and synoptic characteristics is a summary and discussion section that highlights the more notable features of the period. It concludes with an overview of YOTC's plans to leverage these features and events for case-study research to improve our understanding, modeling, and prediction capabilities associated with tropical convection.

BACKGROUND CONDITIONS AND LOW-FREQUENCY VARIABILITY. Some elements of weather and higher-frequency climate variability that are targeted by YOTC depend on characteristics of the conditions set up by lower-frequency climate variability. For example, the spatial characteristics and manifestations of intraseasonal variability (e.g., MJO) can be modified by the conditions of ENSO and the Indian Ocean dipole (e.g., Hendon et al. 1999; Kessler 2001; Waliser et al. 2001; Lau 2005; Hendon et al. 2007; Rao et al. 2007; Ajayamohan et al. 2009). Moreover, these low-frequency tropical climate conditions influence the manifestations of extratropical patterns of atmospheric variability (e.g., Horel and Wallace 1982; Renwick and Wallace 1996; Kumar and Hoerling 1998; Newman and Sardeshmukh 1998; Wallace 2000; Ambaum et al. 2001; Giannini et al. 2001; Hastenrath and Greischar 2001; Ostermeier and Wallace 2003). For these reasons, we begin by documenting the background conditions and evolution of low-frequency climate patterns, including a couple of the more significant extratropical modes of climate variability. Figure 1 shows the anomalous characteristics of sea surface temperature (SST) in the three tropical ocean basins during the YOTC period. Starting with the Pacific, the early half the YOTC period is characterized by modest La Niña conditions, while the latter half is characterized by modest El Niño conditions. Closer examination shows that the 2008/09 boreal winter period is cool and the 2009/10 boreal winter period is warm, both spring-to-summer periods tend to exhibit warming conditions, and the 2008 (2009) boreal fall undergoes cooling (warming) conditions. Overall the largest and longer-lived anomalous conditions tend to be more strongly exhibited in the western half of the Pacific basin compared to the eastern half. This evolution in anomalous SST (i.e. La Niña vs El Niño) between the first half and the second half of the YOTC period represents an excellent contrast for studying its effects on tropical convection characteristics.

For the Indian Ocean, there is some similarity to the Pacific, with a tendency toward cool (warm)

conditions in the first (second) half of the YOTC period, albeit with about half or less the amplitudes exhibited in the Pacific. The characteristics of the Indian Ocean SST, particularly the anomalous east–west temperature gradient across the tropical Indian Ocean, can be linked to a number of important regional climate effects. For example, extreme September–November rainfall in tropical East Africa has been associated with periods when the western (eastern) Indian Ocean SST is anomalously high (low)—meaning a weakening of the normal west-to-east positive SST gradient (Black et al. 2003). Similarly,

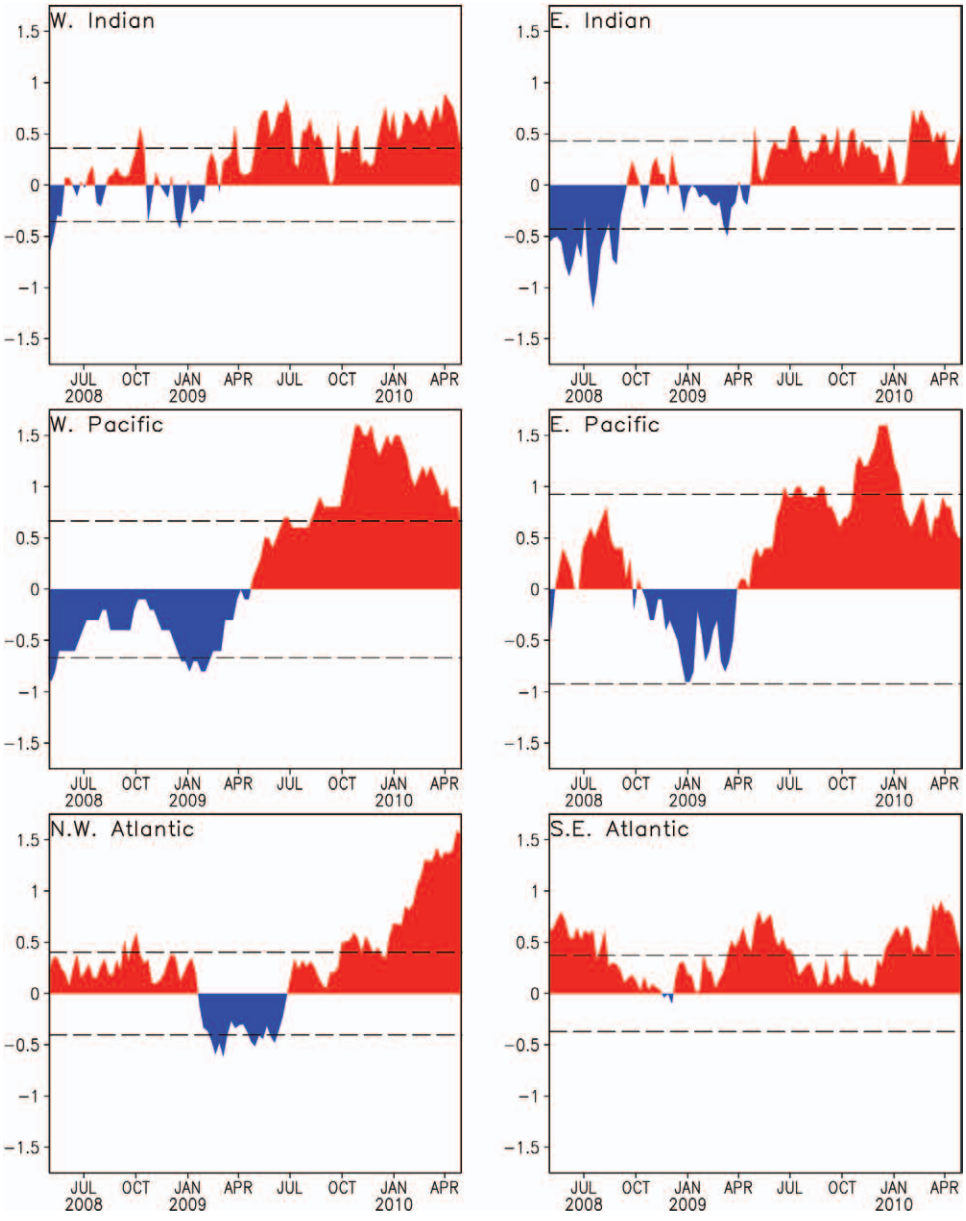

Fig. 1. Tropical ocean SST anomalies (°C) in terms of weekly values during the YOTC period. (top left) West Indian Ocean (10°S–10°N, 50°– 70°E), (top right) east Indian Ocean (10°S– 0°, 90°–110°E), (middle left) west Pacific Ocean (5°S–5°N, 160°E–150°W), (middle right) east Pacific Ocean (5°S–5°N, 150°–90°W), (bottom left) North Atlantic (5°–25°N, 55°–15°W), (bottom right) South Atlantic (20°S–0°, 30°W–10°E). Notes: 1) The west (east) Pacific Ocean defined here is often referred to as Niño-4 (Niño-3); 2) subtracting the east from the west Indian Ocean time series gives the Indian Ocean dipole (IOD) mode index (DMI, not shown; Saji et al. 1999). Time series are from online (tropical Pacific at www.cpc.noaa.gov/data/indices/; other time series are from http://ioc-goos-oopc.org/state_of_the_ocean/).

northward-propagating intraseasonal variability (ISV) has been found to be stronger and more coherent when the western (eastern) Indian Ocean SST is anomalously low (high) (Rao et al. 2007; Ajayamohan et al. 2008, 2009). During most of YOTC, the Indian Ocean warmed, somewhat in concert with the Pacific Ocean. The western Indian Ocean was generally about 0.5°C warmer than the eastern Indian Ocean, indicating that the normal west-to-east temperature gradient in the Indian Ocean was weaker than normal throughout most of YOTC. For the Atlantic, the most remarkable feature is the exceptional warming that develops during the winter of 2009/10, lagging the warming in the Pacific by 3–6 months (Carton and Huang 1994; Enfield and Mayer 1997). This is a peak value when considering the record back to 1982. The southern tropical Atlantic exhibits warm conditions over nearly all the YOTC period, with peak magnitudes typical when considering the most recent three decades (not shown).

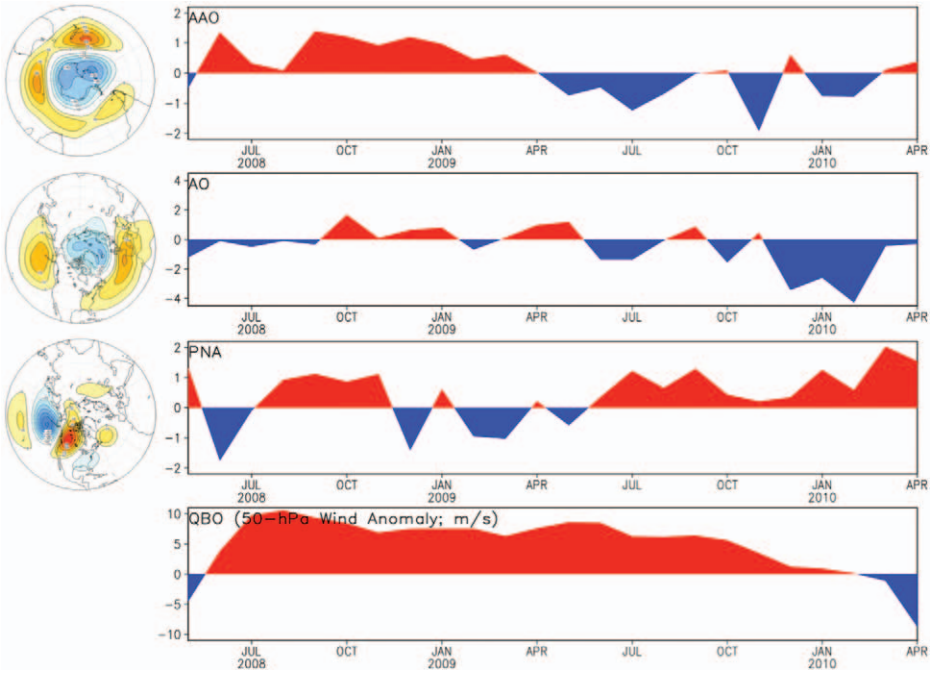

Fig. 2. Monthly time series of (from top to bottom) the AAO, AO, PNA, and the QBO for the YOTC period (unitless, except for QBO in m s^{-1}). To the left of the first three indices are the spatial patterns of the 500-hPa geopotential height anomaly patterns associated with each of the modes of variability; each contour represents 10 m. Indices are defined and the data obtained from the following two Climate Prediction Center websites (www.cpc.noaa.gov/data/indices/, www.cpc.ncep.noaa.gov/products/precip/CWlink/daily_ao_index/teleconnections.shtml). The spatial patterns of the AAO, AO, and PNA were obtained from online (at www.emc.ncep.noaa.gov/gmb/ssaha/).

Figure 2 illustrates the time evolution and spatial patterns (see caption) of three important modes of extratropical variability during the YOTC period. These three extratropical modes include the Pacific–North America (PNA), Arctic Oscillation (AO), and the Antarctic Oscillation (AAO; www.cpc.noaa.gov/data/indices/), and have been shown to be strongly correlated to tropical convection variability and influence low-frequency weather variations (Horel and Wallace 1981; Wallace and Gutzler 1981; Hurrell 1996; Thompson and Wallace 1998; Deser 2000; Thompson and Wallace 2000; e.g., Ambaum et al. 2001; L'Heureux and Higgins 2008; Pohl et al. 2010). The AO exhibits an overall anticorrelation with tropical Pacific and northern tropical Atlantic SSTs shown in Fig. 1, being in mostly a positive (negative) phase during these two oceans' cool (warm) periods. The AAO exhibits a strong anticorrelation to the Pacific SSTs, particularly the western Pacific, while the PNA exhibits a correlation most strongly to the eastern Pacific SSTs. Also illustrated in Fig. 2 is the evolution of the quasi-biennial oscillation (QBO) during YOTC, as indicated by the 50-hPa wind index time series. For the most part, the entire period of YOTC is dominated by a westerly phase of the QBO, with only the very ends of the period being relatively neutral. Finally, to comprehensively describe the background conditions under which the YOTC period evolved, it is worth noting that CO_2 concentration averaged over the 2-yr period was 386.8 ppm with a linear trend of about +2.0 ppm yr^{-1} (mean and least squares trend estimated for YOTC period from ftp://ftp.cmdl.noaa.gov/ccg/co2/trends/co2_mm_mlo.txt), the solar cycle was largely in the minimum phase of the 11-yr cycle (www.swpc.noaa.gov/SolarCycle/), and there was no significant volcanic activity that occurred in or near the tropics.

TROPICAL WAVES. *Madden–Julian oscillation.* The MJO is of considerable interest in YOTC due to the considerable influence it has on other components of our weather and climate system, including monsoon onset and breaks, TCs, ENSO evolution, extratropical variability, etc. (Madden and Julian 1971; Zhang 2005; Lau and Waliser 2011). An overview of MJO-related tropical convective variability that occurred during the YOTC period is provided in Fig. 3. This figure uses satellite outgoing longwave radiation (OLR) data filtered for eastward-propagating wavenumbers 1–5 and periods 30–96 days as a proxy for the convective variability associated with the MJO (Wheeler and Kiladis 1999; Wheeler and Weickmann 2001). Six cases of relatively strong MJO activity have been identified during this period (see Figs. 3a–f). By this measure, the three strongest cases of enhanced convection (i.e., negative OLR anomalies) associated with the MJO during YOTC were in April 2009 (Fig. 3d), November 2009 (Fig. 3e), and January 2010 (Fig. 3f). These periods of MJO activity also show as being the strongest, although with different relative magnitudes, when viewed using the real-time multivariate MJO index (Wheeler and Hendon 2004), which includes lower- and upper-tropospheric zonal winds in the MJO definition. Placing this activity into a historical context, the YOTC MJO cases were weaker than those that occurred in 8 of the previous 12 yr, very much weaker than the very strong MJO activity that occurred in the lead up to the 1997 El Niño, and a little weaker than the well-documented activity that occurred during TOGA COARE (not shown).

Highlighting the more notable cases, the *May–June 2008 (Fig. 3a)* case involved modulation of convective activity over much of the tropics, including an enhancement of convection over the western Indian Ocean in late May (which approximately coincided with the start of the first northward propagation of intraseasonal convection into India of the 2008 monsoon season shown later in Fig. 8), as well as an enhancement of convection in the eastern Pacific ITCZ (as was associated with the development of several TCs). The *April–May 2009 (Fig. 3d)* case included nearly two complete cycles of the MJO. The first exhibited strong interaction with other equatorial waves (see first case in the "Convectively coupled equatorial

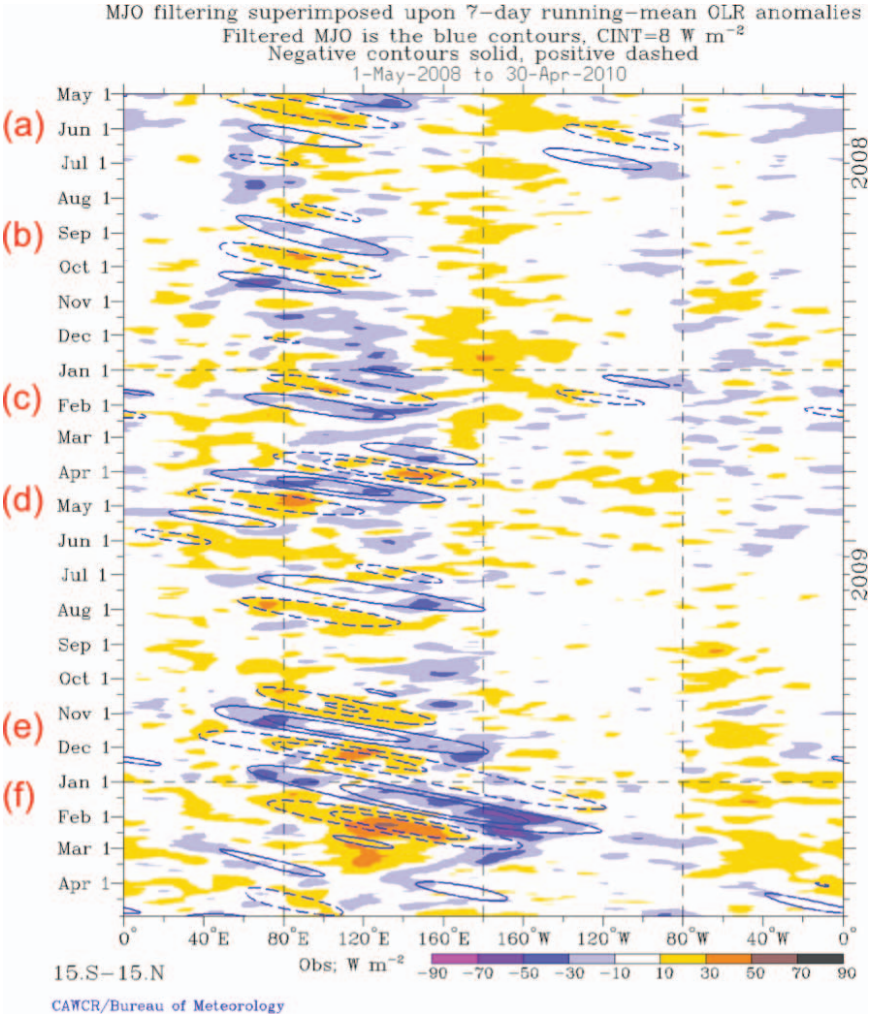

Fig. 3. Time–longitude diagram of 15°S–15°N-averaged OLR anomalies (W m^{-2}) during the YOTC period, with MJO-filtered OLR anomalies superimposed. Shading is for "total" OLR anomalies that have been temporally (7-day running mean) and spatially (R21 spectral truncation) smoothed. Contours show OLR that has been wavenumber–frequency filtered for eastward-propagating waves 1–5 and periods 30–96 days, as is used to signify convective variability associated with the MJO. Contour interval is 8 W m^{-2}, with dashed contours used for positive MJO-associated OLR anomalies. Labels (a)–(f) refer to the identified cases of MJO activity.

waves" section) and has been implicated in the shift to El Niño conditions through the enhancement of westerly surface wind anomalies across the Pacific (once convection reached the Pacific in late April). The second cycle was associated with the first northward propagation of intraseasonal convection into India for 2009 (see Fig. 8). The *October–December 2009 (Fig. 3e)* case began with suppressed convection over the near-equatorial Indian Ocean in mid-October, followed by a switch to enhanced convection over Africa and the western Indian Ocean, which progressively gained in strength until peaking in the second week of November, with the strongest negative OLR anomalies observed for the near-equatorial Indian Ocean for the whole of the YOTC period. Finally, for the *December 2009–February 2010 (Fig. 3f)* case, enhanced convection reached farther eastward than any other MJO of the YOTC period, presumably helped by the warm Pacific conditions. The MJO cases discussed above, including the nuances of their initiation, propagation, possible connections, and influences on TC formation, make them excellent cases for broadening our understanding of multiscale interactions as well as for model verification studies.

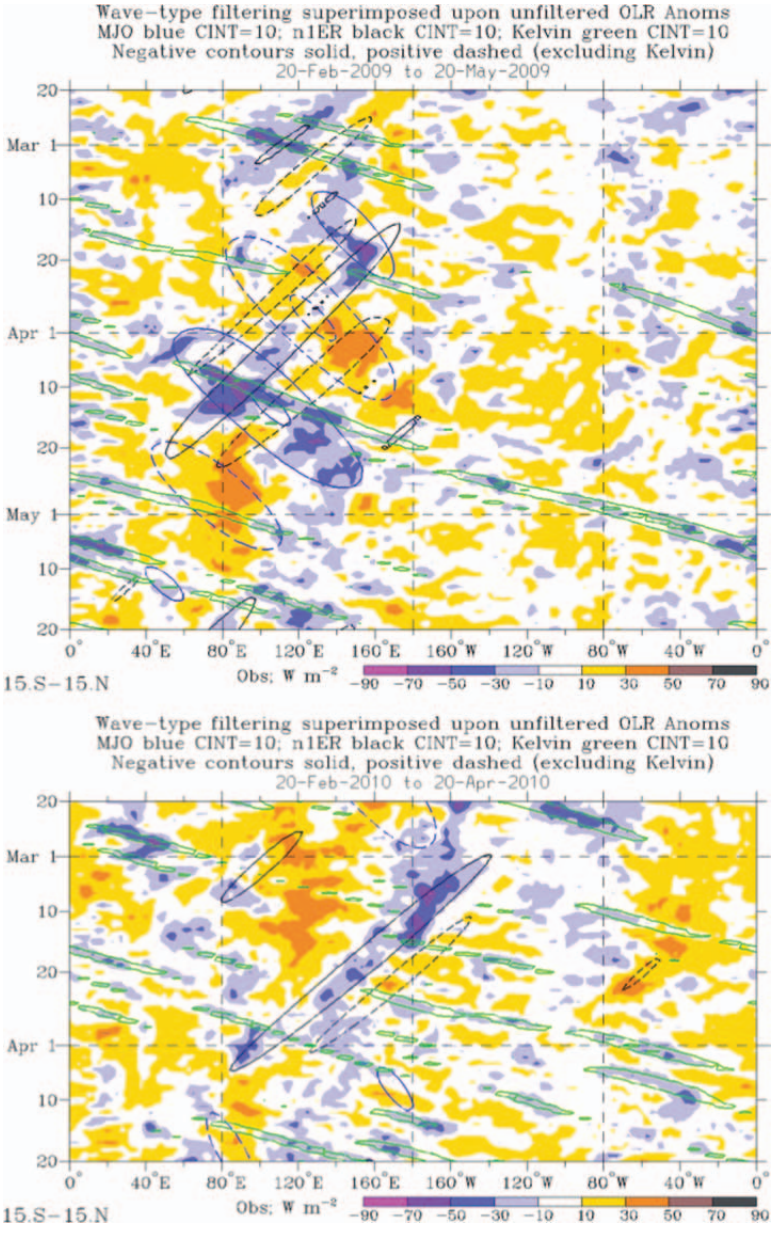

Fig. 4. (top) 15°S–15°N-averaged OLR anomalies (W m^{-2}) for the period 20 Feb–20 May 2009, during which multiple interacting waves (MJO, equatorial Rossby, and Kelvin) existed (CCEW case 1). Shading is for the unfiltered OLR anomalies, blue contours for the MJO-filtered OLR anomalies, black contours for the *n* = 1 ER wave filtering, and green contours for the Kelvin wave filtering. Contour interval is 10 W m^{-2}. Positive contours for the MJO and ER wave anomalies are dashed, whereas the Kelvin wave the positive contours are omitted. (bottom) As in (top), but for the period 20 Feb–20 Apr 2010 (CCEW case 2).

Convectively coupled equatorial waves. Here we focus on just two periods of notable occurrences of CCEWs (Takayabu 1994; Wheeler and Kiladis 1999; Kiladis et al. 2009). The first case involves multiple interacting waves during the period March–April 2009 (Fig. 4, top). The MJO, (*n* = 1) equatorial Rossby (ER), and Kelvin waves were all simultaneously active, seemingly propagating through each other to account for the observed complex behavior of simultaneous eastward and westward propagation. For example, the enhanced convection that occurred near 90°E on 10 April appears to be a result of the superposition of the influence of all three waves propagating at different speeds and/or directions. The ER wave in this example originates from an earlier convective blowup that occurred well to the east about 20 days previously. The Kelvin wave, in contrast, originates from the Atlantic, crossing 0° on about 2 April. A later strong Kelvin wave

crossed the Atlantic and Africa in the first week of May.

The second case involves coherent westward movement of convection from east of the date line in the Pacific to the Indian Ocean during March 2010 (Fig. 4, bottom). Consistent with the structure of an $n = 1$ ER wave, this convection was mostly symmetric about the equator and occurred in conjunction with cyclonic circulation cells on either side of the equator. Imbedded within these cyclonic circulation cells were several TCs: TCs Tomas and Ului in the Southern Hemisphere and TC Omais (Agaton) in the Northern Hemisphere. TC Ului followed a long westward track, from ~170°E on 10 March to ~150°E on 21 March. In addition, prominent Kelvin wave activity was observed during this case period (green contours in Fig. 4). These cases, and others like them, represent stringent tests for our global models to properly represent and as of yet little attention has been paid to the verification of CCEW activity nor to the metrics used for the evaluation (see M12).

Easterly waves. As with the waves discussed above, easterly waves (EWs) play a key role in modulating tropical cyclogenesis, and are most prevalent during the Northern Hemisphere summer over West Africa and the tropical Atlantic (Reed et al. 1977; Kiladis et al. 2006) as well as the Pacific (Reed and Recker 1971; Nitta and Takayabu 1985; Serra et al. 2008). Figure 5 shows the July–September variance of Tropical Rainfall Measuring Mission (TRMM) 3B42 precipitation rate (Huffman et al. 2007) in the "tropical depression" (TD) wavenumber frequency band (wavenumber −20 to −6 and period 2–5 days). Note that TCs may contribute to the TD-band variance, especially in the western Atlantic and Pacific Oceans, north of 15°N. The top panel is indicative of climatological EW storm tracks (Thorncroft and Hodges 2001). The middle panel shows that 2008 was characterized by anomalously high TD variance in the West African and tropical Atlantic region. The region of maximum TD variance (6°–15°N, 50°W–15°E) was 13% higher in 2008 than climatology. In contrast, TD variance in 2009 was 5% lower than climatology over the same region (Fig. 5c). In 2008, TD variance was 20% below the 1998–2009 mean over the region 6°–15°N, 150–80°W. Anomalously low TD variance was especially prominent in the central Pacific, consistent with the negative SST anomalies there (see "Background conditions and low-frequency variability" section), whereas TD variance was 28% above climatology in 2009 over the same region,

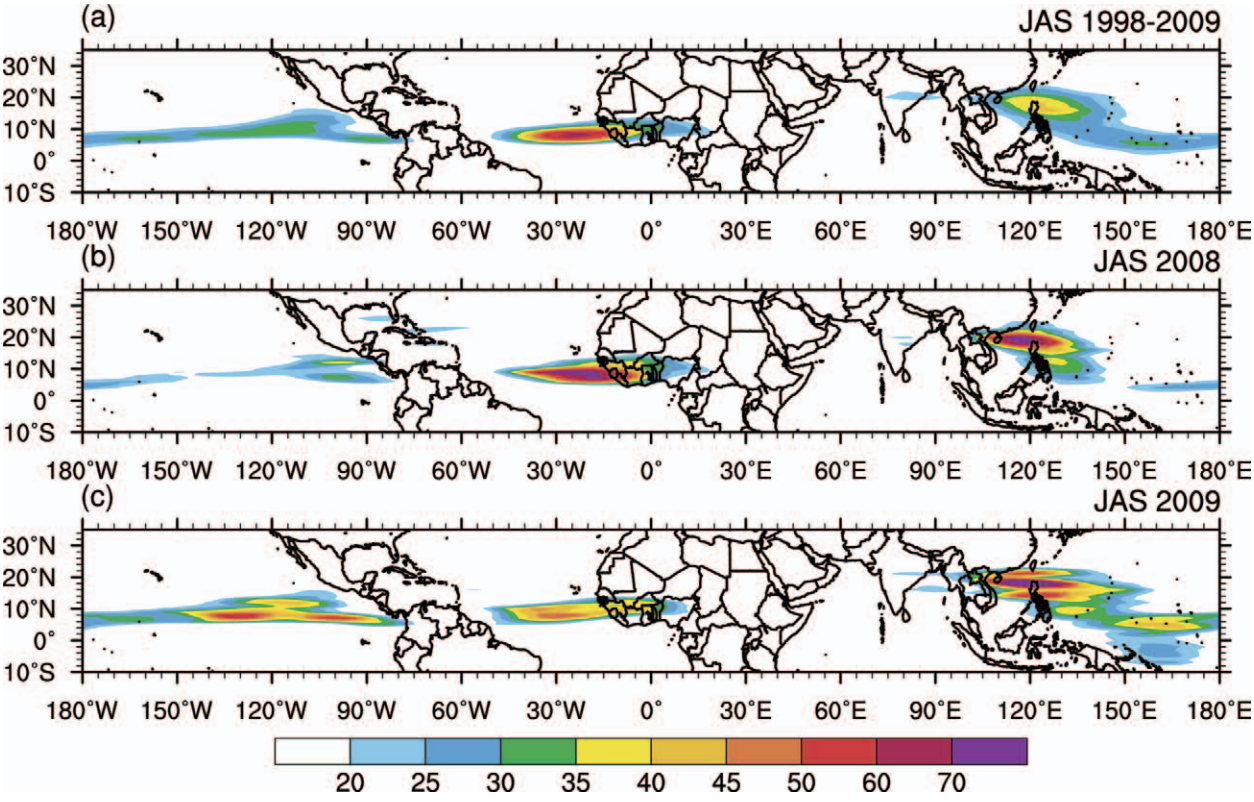

Fig. 5. Variance of TRMM 3B42 TD-filtered rain rate [(mm day^{-1})^2] for Jul–Sep averaged over (a) 1998–2009 (b) 2008, and (c) 2009.

consistent with the presence of above-average SSTs. Similarly, west Pacific TD-band variance was also enhanced in 2009 (Hsu et al. 2009). The relationship between the contrasting EW activity in 2008 and 2009, ENSO, and ISV associated with the MJO and CCEWs, including how these vary with boundary forcings, is an area of research that could benefit from the YOTC. It will also be important and interesting to contrast the EW variability observed in the YOTC years with that observed during the 2006 African Monsoon Multidisciplinary Analyses (AMMA) field campaign over West Africa (Redelsperger et al. 2006; Janicot et al. 2008).

Figure 6 provides a more detailed look at the tracks and characteristics of easterly waves during July–September 2008 and 2009. The Hovmöller diagrams include precipitation rate and objectively determined EW tracks based on 700-hPa vorticity maxima (Janiga 2010). The period between mid-July and early September 2008 was associated with numerous intense African EWs moving over tropical North Africa into the east Atlantic. Consistent with past EW composite studies [see Kiladis et al. (2006), and references therein], the peak precipitation rate is located ahead of the EW tracks or in the northerlies over Africa (Fig. 6). A closer examination of the most intense waves reveals that mesoscale convective systems formed northwest of the midlevel trough and then moved southwestward but remained fairly coupled to the wave. One example of this is an EW that moved from the Ethiopian highlands to the east Atlantic between 14 and 22 July 2008 (see dashed box in Fig. 6a). Both this wave and the preceding wave contributed to heavy rainfall and flooding in West Africa with rainfall totals between 17 and 21 July in excess of 4 cm over much of West Africa and rainfall totals exceeding 10 cm in Burkina Faso and Liberia. Another high-impact event occurred on 1 September 2009 (see dashed box in Fig. 6b) when an mesoscale convective system, tightly coupled to the

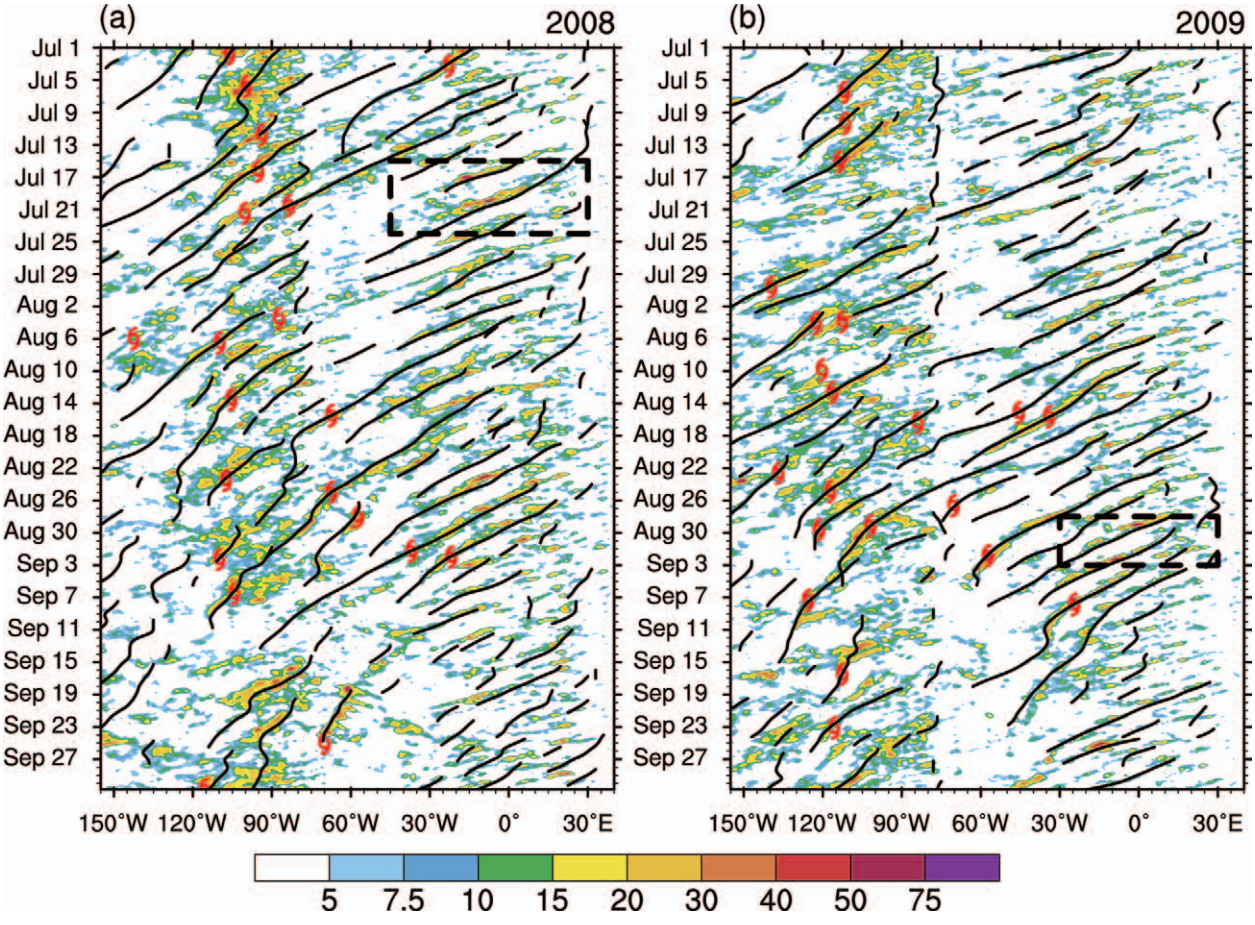

Fig. 6. Hovmöller diagram of TRMM 3B42 rain rate (mm day^{-1}, shaded) averaged between 5° and 20°N and objective tracks of vorticity centers exceeding 1 × 10^{-5} s^{-1} observed between 0° and 30°N for (a) 2008 and (b) 2009. The time and longitude of named storm genesis is indicated by the red markers. Dashed boxes highlight periods of high-impact weather referred to in the text.

midlevel trough of an EW, produced 263 mm of rainfall in Ouagadougou, Burkina Faso, according to rain gauges (not shown). Examinations of the relationship between subsynoptic aspects of the structure of the EWs and these convective systems would be greatly aided by the high resolution of the YOTC analyses.

TROPICAL CYCLONES. TCs are by far one of the most significant manifestations of organized tropical convection, notably because of their sheer elegance as a physical system but also because of the societal need for ever-increasing accurate predictions of their strength and track. Climatologically speaking, the last several years have been remarkably below average in terms of overall global tropical cyclone activity. Since the previous peak in overall global and Northern Hemisphere accumulated cyclone energy (ACE) in 2005, tropical cyclone activity has significantly decreased, especially over the entire Pacific with the 2008/09 YOTC "year" having the lowest global ACE since 1977 (Maue 2009, 2011). Despite YOTC occurring within a historically quiet period relative to the last three decades, there were still ample TCs that developed, with some particularly unique cases and conditions.

The tracks of all TCs during the YOTC period are illustrated in Fig. 7, with those mentioned below annotated with a number at the start and end of the track. In 2008, the western North Pacific (WNP) had 25 tropical storms with 12 becoming typhoons—a season with slightly below-normal activity. Typhoon Jangmi (Fig. 7a—track 1) was the strongest TC of

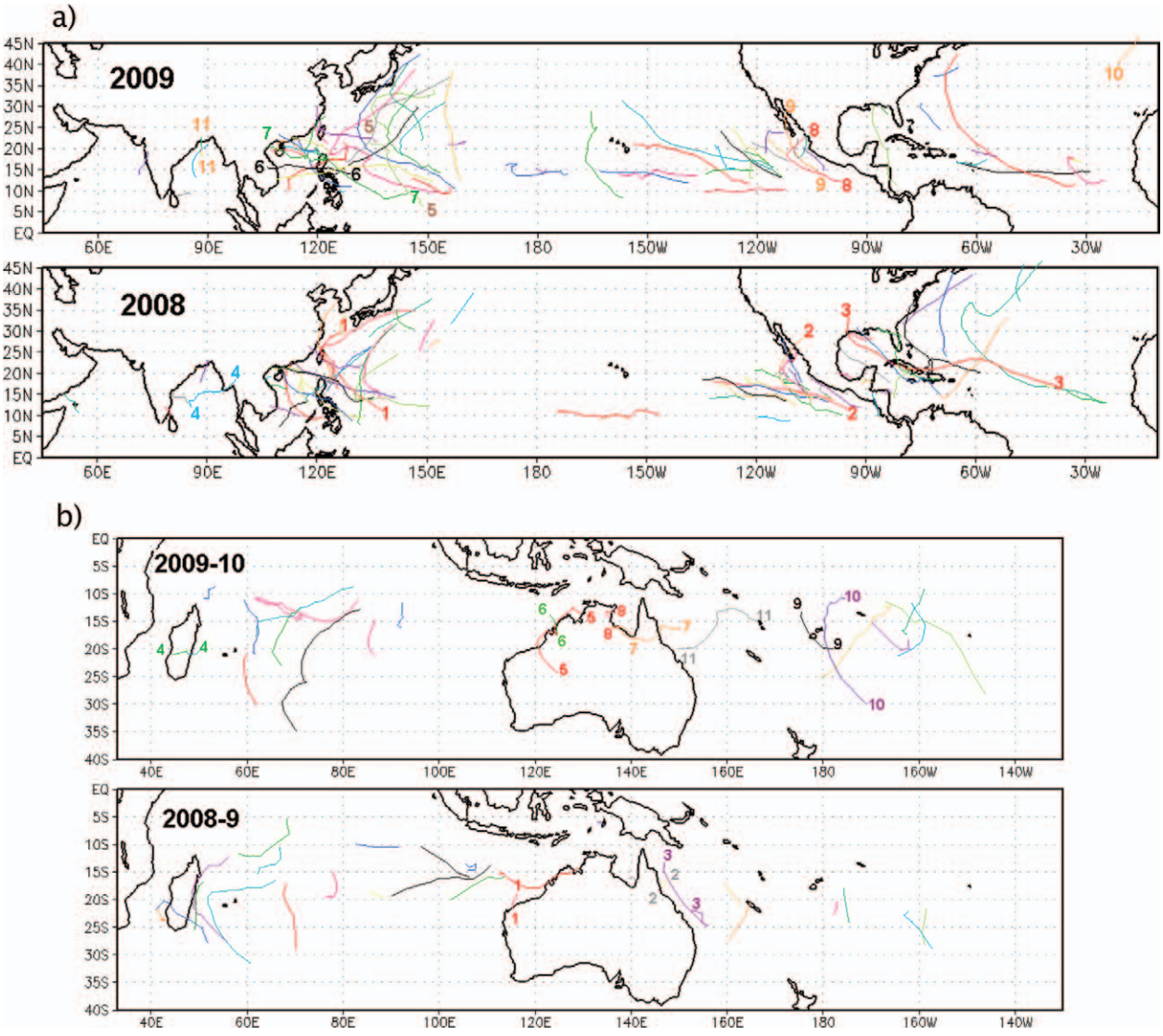

Fig. 7. (a) Northern Hemisphere TC tracks: (top) 2009 and (bottom) 2008. (b) Southern Hemisphere TC tracks: (top) 2009/10 and (bottom) 2008/09. Numbers refer to specific storms discussed in the text (see "Tropical cyclones" section).

the season across the whole Northern Hemisphere with sustained winds of 145 kt. Unusually, Japan received no direct landfalls during this season. The eastern North Pacific exhibited activity close to normal. Hurricane Norbert (Fig. 7a—track 2) was the strongest of the season and was also one of three TCs (with Julio and Lowell) to make landfall over Mexico. The North Atlantic was active; for the first time, major hurricanes (winds of 100 kt or more) occurred in each of the 5 consecutive months from July to November. Hurricanes Fay, Gustav, Ike, and Paloma all hit Cuba. Ike (Fig. 7a—track 3) was one of the largest storms (in aerial size) ever recorded in this basin and caused a storm surge of up to 7 m along the Gulf of Mexico coast. In the north Indian Ocean, the most significant storm was Cyclone Nargis (Fig. 7a—track 4), which made landfall over Myanmar and caused a huge storm surge up the Irrawaddy delta. This resulted in the loss of as many as 100,000 lives. During the 2008/09 Southern Hemisphere season, four storms brought heavy rainfall to Madagascar. Cyclones Dominic and Ellie (Fig. 7b—tracks 1 and 2) made landfall over the Australian coast, while the strongest storm of the season, Hamish (Fig. 7b—track 3), kept just offshore of the Australian east coast.

During the 2009 Northern Hemisphere season, the El Niño event induced stronger typhoons in the western North Pacific and the storm tracks tended to originate farther east into the central parts of the Pacific Ocean. The strongest typhoon of the season, Nida (Fig. 7a—track 5), peaked with sustained winds of near 160 kt. Notable events were Typhoon Ketsana (Fig. 7a—track 6), which caused extensive flooding in the Philippine capital Manila and later across Vietnam and Cambodia, and slow-moving Typhoon Parma (Fig. 7a—track 7), which dumped an estimated 1.8 m of rain over the northern Philippines. The El Niño event also resulted in higher-than-normal activity in the eastern and central North Pacific. Hurricane Rick (Fig. 7a—track 8) became the second strongest east Pacific hurricane on record, making landfall over Mexico, as did Hurricane Jimena (Fig. 7a—track 9). In the North Atlantic, the El Niño event resulted in a quiet season for the Caribbean and United States. The most unusual event of the season was high-latitude Tropical Storm Grace (Fig. 7a—track 10), which developed near the Azores and eventually tracked across the United Kingdom as an extratropical system. In the north Indian Ocean, Tropical Storm Aila (Fig. 7a—track 11) caused a storm surge of up to 3 m across Bangladesh, which resulted in hundreds of fatalities in this region. The most notable events for the 2009/10 Southern Hemisphere season included Tropical Storm Hubert (Fig. 7b—track 4), which caused significant disruption over Madagascar. While activity was quiet around Australia, several storms [Laurence, Magda, Olga, and Paul (Fig. 7b—tracks 5–8, respectively)] impacted coastal regions. Both Mick and Tomas (Fig. 7b—tracks 9 and 10, respectively) affected Fiji, and Ului (Fig. 7b—track 11) was the strongest South Pacific cyclone for 5 yr. To round off the season, a highly unusual tropical storm in the South Atlantic developed in March 2010 and was named Anita by Brazilian meteorological organizations (not shown). It was the first such storm to develop in this region since Catarina in 2004; although unlike Catarina, Anita posed no threat to land.

TC research in YOTC benefits from the occurrence of the THORPEX Pacific Asian Regional Campaign (T-PARC) and Tropical Cyclone Structure 2008 (TCS-08) field experiments that conducted multiple aircraft operations into Typhoons Nuri, Sinlaku, Hagupit, and Jangmi. The science objectives of these campaigns included increasing understanding of TC formation, structure and intensity change, extratropical transition, and the value of targeted observations. In particular, analysis of aircraft observations are being conducted with reference to gridded YOTC analysis fields provided by the European Centre for Medium-Range Weather Forecasts (ECMWF).

MONSOONS. The monsoons exhibit considerable breadth in terms of the phenomena and range of space and time scales associated with tropical convection (e.g., Ramage 1971; Murakami 1975; Gadgil 1981; Lau and Lim 1982; Hastenrath 1987; Trenberth et al. 2000; Rodwell and Hoskins 2001; Wang 2006). This includes seasonal and planetary-scale changes in the atmospheric and ocean circulations, a preponderance of tropical wave activity, modulations of TCs' other synoptic scales, and diurnal variations. The monsoons represent highly integrating features of tropical convection and remain an ominous forecast challenge from not only their onset but for subsequent breaks and active periods, extreme events, and seasonal totals. Here, we highlight some of the notable monsoon characteristics during the YOTC period.

Indian. With the 2008 Indian summer monsoon being "normal," garnering 98% of long-term average all India rainfall (AIR), and 2009 being one of the worst drought over the past century with AIR being 22% below the long-term average, the YOTC period provides a unique opportunity to examine and unravel differences in propagation characteristics and

structure of the monsoon intraseasonal oscillations (MISOs) and how they lead to interannual variability. Evolution of the daily rainfall over India (between 6° and 27°N and 72° and 85°E) indicates (Fig. 8) that the near-normal monsoon of 2008 had three strong, active spells of rainfall and only two weak breaks, while the severe-drought monsoon of 2009 was characterized by three long breaks and two weak active spells. This is consistent with some recent studies (Joseph et al. 2010) indicating that long breaks are characteristic features of Indian monsoon droughts. The monsoon onset over Kerala (MOK) during 2008 occurred on 31 May, close to the climatological date. Although 2009 was a drought year, the onset took place on 23 May, a week before the normal onset date, consistent with earlier findings that MOK has no relationship with the performance of the monsoon.

Significant differences in ISV during 2008 and 2009 are noteworthy (Figs. 8c–f). The time–latitude diagrams of 30–60-day filtered OLR anomalies averaged over Indian longitudes show that the northward propagation of MISO was slower during 2008 compared to that during 2009. Also, consistent with the daily rainfall (Figs. 8a,b), the MISO during 2008 was characterized by three wet and two dry northward-propagating spells, while during 2009 there were

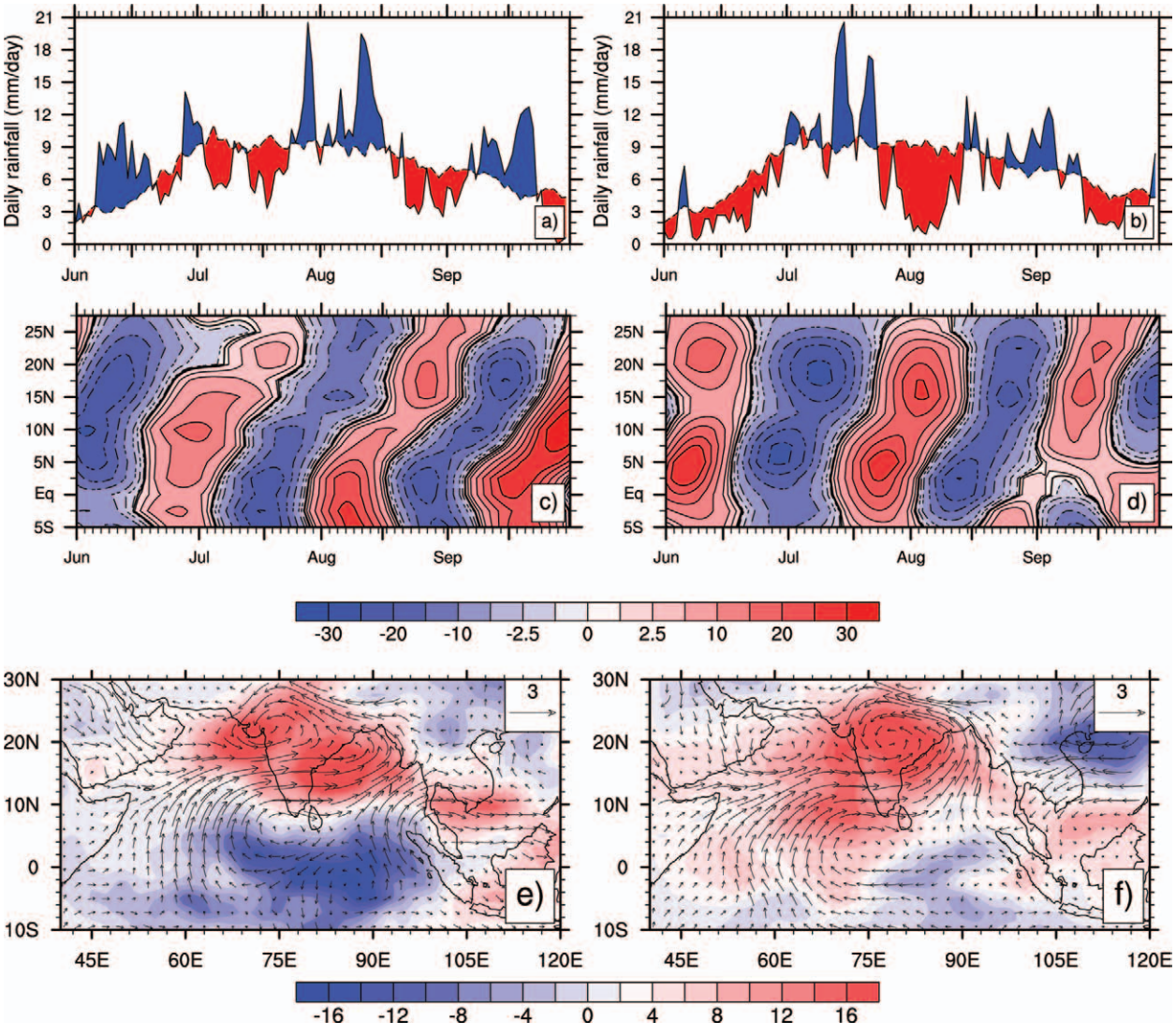

Fig. 8. (a) Daily rainfall (mm day^{-1}) over India (averaged between 72° and 85°E and 6° and 27°N) during 1 Jun–30 Sept 2008. Above (below)-normal rainfall is shown in blue (red) on either side of the daily climatology. (b) As in (a), but for 2009. (c) Northward propagation as seen from 30–60-day filtered OLR anomalies (W m^{-2}) averaged over 60°–90°E during 2008. (d) As in (c), but for 2009. (e) Lag-zero regressed structure of 10–90-day filtered OLR (shaded) and 850-hPa winds with respect to a reference time series (filtered OLR anomalies averaged over central India) during 2008. (f) As in (e), but for 2009.

two wet and three dry spells. Another important feature (Figs. 8b,d) is the intensity of the long break during August 2009 that contributed to the severity of the drought of the year. What was responsible for this intense long break during 2009? Neena et al. (2011) show that an interaction between a westward-propagating planetary-scale equatorial Rossby wave and the northward-propagating MISO may have been responsible for this intense long break. The characteristic spatial pattern associated with the MISO during the 2 yr also had notable differences. Regressed 10–90-day filtered OLR and winds at 850 hPa with respect to a reference time series (filtered OLR averaged over central India) show a canonical convectively coupled monsoon ISV structure with a meridional dipole in OLR over Indian longitudes during 2008 (Waliser 2006; Goswami 2011). During 2009, the meridional dipole structure of convection is conspicuously absent, leading to a much larger meridional scale for low-level winds during 2009 compared to 2008. Understanding what is responsible for the differences in propagation characteristics and spatial structure of ISV between these 2 yr is crucial for developing the ability to forecast them at lead times of 2–3 weeks, and is a major challenge for YOTC.

East Asian/western North Pacific. As with the Indian monsoon, the July–September seasonal-mean low-level circulation and convective activity in the East Asian/WNP (EA/WNP) monsoon region were distinctly different between 2008 and 2009. During July–September 2008, the monsoon trough was weaker than normal and confined mostly in the South China Sea, while the ridge was unusually strong and occupied the whole WNP from the equator to 50°N (Fig. 9). Rainfall was above normal for most of the WNP, and in particular in the tropics from the South China Sea all the way to the date line. The stronger monsoon trough and more rainfall were likely induced by the 2009 El Niño, which became mature in early summer (e.g., Lau and Nath 2006). In contrast, the monsoon trough was stronger and extended farther eastward than normal in July–September 2009, while the ridge shifted more northward than usual. The corresponding circulation was characterized by a cyclonic anomaly in the South China Sea and the Philippine Sea and anticyclonic anomaly in the extratropical WNP. Moreover in 2009, the tropical EA/WNP from the South China Sea to 150°E was dominated by a westerly anomaly. As a result, rainfall was above normal for most of the WNP, and in particular in the tropics from the South China Sea all the way to the date line.

Percentile maps show how anomalous the rainfall and specific humidity were during YOTC. The 850-hPa specific humidity was generally above the 85th percentile in the WNP west of 140°E but lower than the 15th percentile east of 160°E in the prevailing region of the unusually strong subtropical ridge. Extremely low rainfall (below the 10th percentile) was observed in the region between 5° and 15°N and east of 140°E where the anticyclonic circulation and easterly anomaly prevailed. In July–September 2009, the high specific humidity region extended frther eastward and occupied almost the whole tropical and subtropical EA/WNP region. While rainfall was above the 50th percentile throughout most of this region, it was generally not as extreme as in specific humidity, except in the central rainfall-abundant areas, where it exceeded the 90th percentile. Extremely low rainfall was found east of Taiwan and south of Japan and in the subtropical WNP east of 160°E, in all cases where the anticyclonic anomalies prevailed. Note that typically July–September rainfall in the WNP is largely contributed by tropical cyclones, and this appears to be the case for the rainfall and TC distributions in 2008 and 2009 (see Fig. 7). The characteristics mentioned above emphasize the multiscale nature of tropical convection and the interactions between synoptic- and finer-scale convection, the large-scale circulations (e.g, monsoons and CCEWs), and basin-scale climate (e.g., ENSO).

Australian. The YOTC period covers two wet seasons in northern Australia that occur in austral summer. Figure 10 shows a daily time series of rainfall together with the climatological rainfall distribution at Darwin (blue line). Significant intraseasonal variability is exhibited, some of which may be attributed to the MJO (see "Madden–Julian oscillation" section). However, tropical cyclones also contributed significantly to Darwin rainfall, namely, TC Billy (December 2008), TC Lawrence (December 2009) and ex-TC Paula (March 2010) (see "Tropical cyclones" section; Fig. 7), as did a monsoonal low during late February 2010 and long-lived continental squall lines during late October 2009.

Through the development of an objective technique to better characterize the state of the north Australia wet season on any given day, Pope et al. (2009) showed that it is important to consider the entire wet season rather than just the embedded shorter monsoon period. This is because a significant fraction of the rainfall occurs outside the traditionally defined monsoon period. The state analysis technique involved the identification of five wet-season regimes

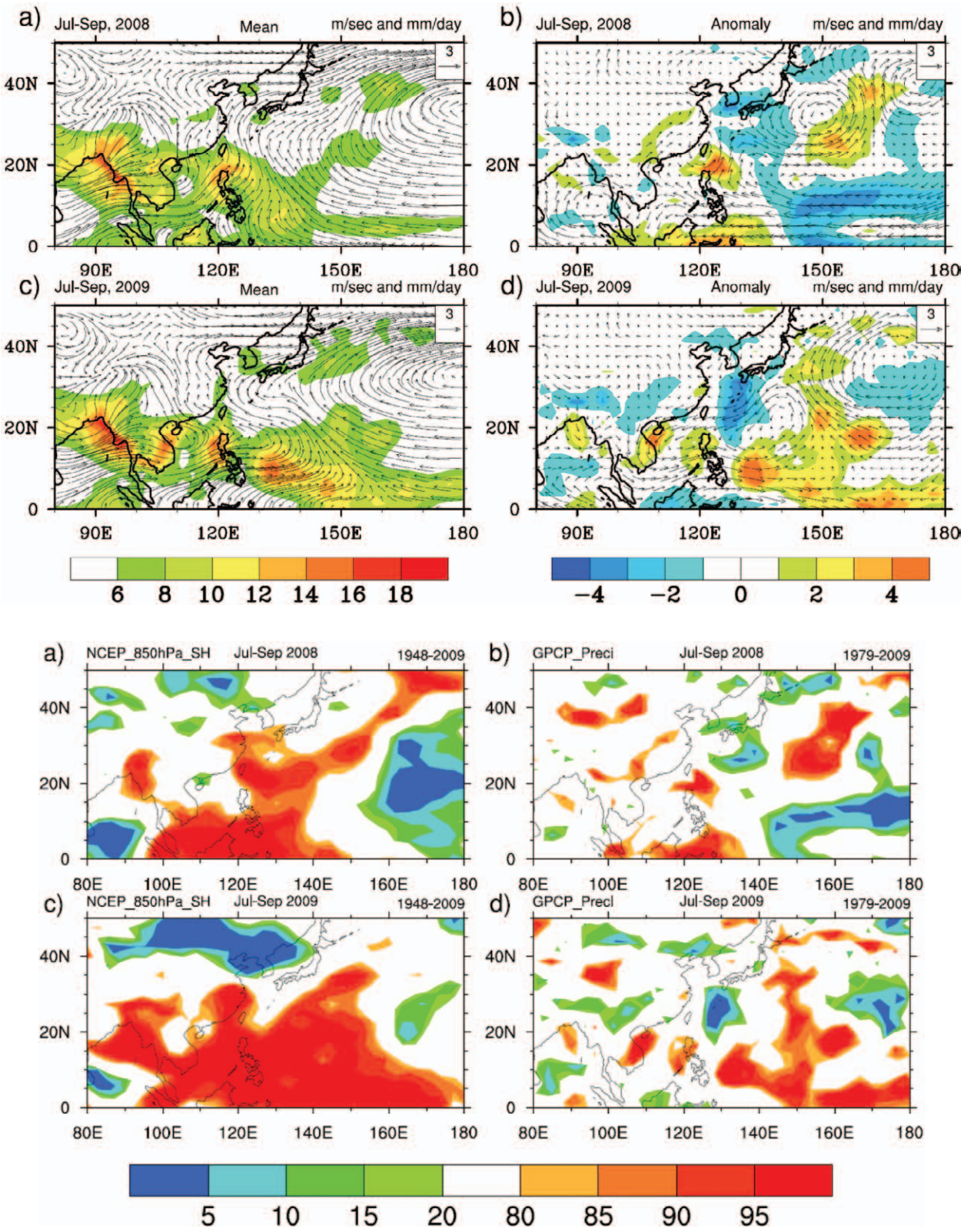

Fig. 9. (top) Rainfall (mm day^{-1}) and 850-hPa wind (m s^{-1}) in Jul–Sep (a) 2008 and (c) 2009. (b),(d) As in (a),(c), but for anomaly. (bottom) Distribution of percentile for (a),(c) 850-hPa specific humidity and (b),(d) rainfall anomalies in Jul–Sep (a),(b) 2008 and (c),(d) 2009. Base periods for calculating percentile are based on trying to the use as long a record as possible for the given dataset selected, thus 1949–2009 and 1979–2009 for specific humidity and rainfall, respectively.

from daily radiosonde data at Darwin. Three of the regimes, termed *deep west*, *moist east*, and *shallow west*, are typically associated with rainfall, where deep west identifies the active phase of the monsoon and moist east signifies monsoon buildup, break, and retreat conditions. Two of the five regimes (east and dry east) represent generally dry conditions. The wet-season onset can be identified by the first significant consecutive days of the moist east regime, and monsoon onset is related to the first occurrences of the deep west regime. Likewise the retreat of the monsoon and the end of the wet season can be determined as the last days of the deep west and moist east regimes, respectively. Figure 10 shows the daily identification of wet-season regimes as described above for the two north Australia wet seasons within YOTC. Also shown are the climatological monsoon onset and retreat days (vertical dashed lines) and the monsoon onset and retreat days for the two seasons (arrows).

Using the moist east regime as an indicator, the 2008/09 wet season started in early November and lasted until mid-March. In contrast, the 2009/10 wet season started in early December and lasted well into April. This is consistent with La Niña conditions in 2008/09, which promote an early wet-season onset (Nicholls et al. 1982; Drosdowsky 1996), while the slight El Niño event in 2009/10 favored a later wet-season onset. Using the definitions above, the onset in 2008 and 2009 occurred on 18 December and 15 December, respectively, close to the mean onset date 19 December (Pope et al. 2009). The retreat of the monsoon in 2008 and 2009 occurred on 17 February 2009 and 5 March 2010, respectively. Hence, the 2008/09 monsoon season was relatively short, while the 2009/10 season was of more or less average length, and the wet season as whole lasted significantly longer than in 2009/10 than in 2008/09.

North American. By measures such as all-Mexico June–August total rainfall, the 2008 North American monsoon (NAM) was the largest since 1941. Positive rainfall anomalies in gauge data (not shown) and negative peak season (July–August) OLR anomalies (Fig. 11a) were exhibited in nearly all regions of Mexico and throughout much of the U.S.-Mexico border region. Consistent with previous studies (Higgins et al. 1998; Castro et al. 2001; Gochis et al. 2007; Liebmann et al. 2008), antecedent SST conditions appear to have played a significant role in the development of this anomaly. Weakening wintertime La Niña conditions (Figs. 11c, 1) in the central and western Pacific, and an extended wintertime drought and warm surface temperatures over western Mexico and the Southwest United States helped initiate an early, robust onset to the NAM in mid-to-late June. Regional precipitation-tracking indices developed as part of the North American Monsoon Forecast Forum (Gochis et al. 2009) showed all NAM regions experiencing anomalously high precipitation accumulations through July. Persistent diabatic heating from convective activity (inferred from negative OLR anomalies) and a northwestward shift in the 200-mb height field (Fig. 11e) during July and August helped provide a favorable pattern for sustained low-level moisture advection (not shown) from the Gulf of California, tropical eastern Pacific, and the Gulf of Mexico into the NAM region (Higgins et al. 2004). As mentioned in the tropical cyclones section, owing to favorable steering

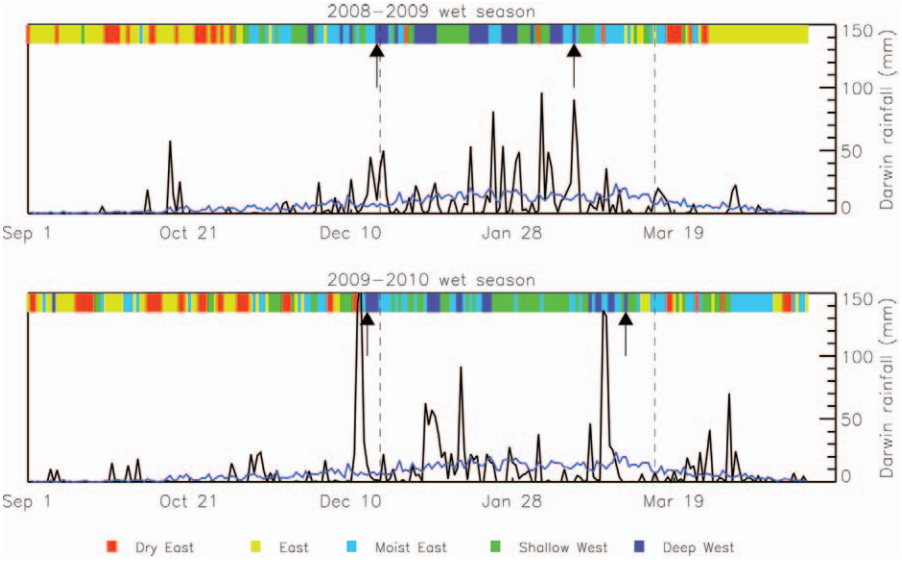

Fig. 10. Time series of daily rainfall (mm; black line) and daily wet-season regime (color bar) for the northern Australia wet seasons of (top) 2008/09 and (bottom) 2009/10. Also shown are the climatological rainfall distribution (blue line), the climatological monsoon onset and retreat days (vertical dashed lines), and the respective season's monsoon onset and retreat days (arrows) as defined in Pope et al. (2009).

circulations, landfalling and near-shore tropical storms also made significant contributions to rainfall totals during July–September of 2008. Englehart and Douglas (2001), Wang et al. (2008) and Serra (2009) each note that circulation patterns favorable for sustaining NAM rainfall are also likely to steer tropical

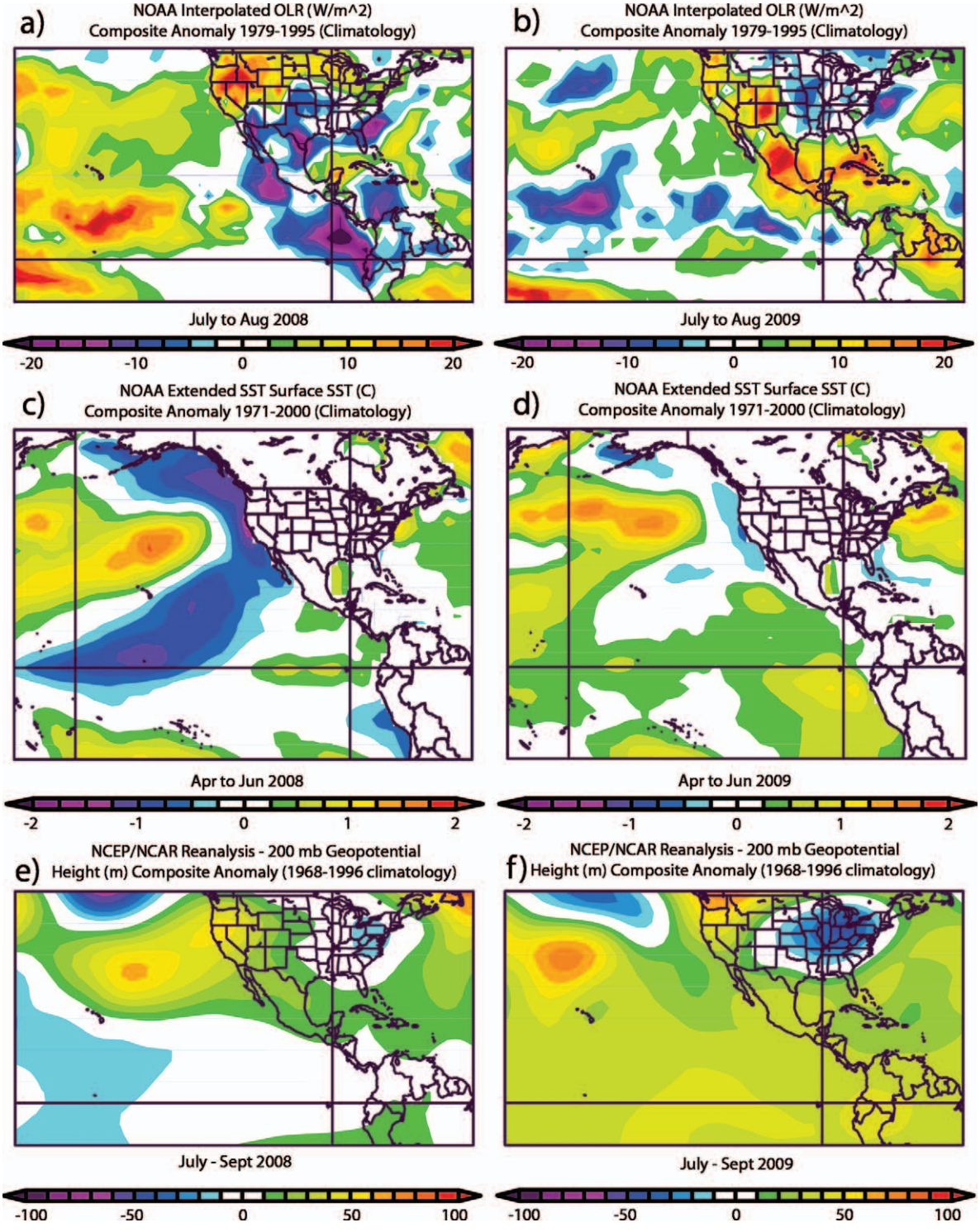

Fig. 11. (a),(b) Jul–Aug National Oceanic and Atmospheric Administration (NOAA) interpolated OLR anomalies (W m^{-2}),(c),(d) antecedent season (Apr–Jun) NOAA extended optimal interpolation (OI) SST anomalies (°C), and (e),(f) Jul–Sep NCEP–National Center for Atmospheric Research (NCAR) reanalysis 200-hPa geopotential height anomalies (m) for 2008 and 2009, respectively.

storms into Mexico, the southwestern United States, Baja California, and the Texas Gulf Coast. Thus, for a year like 2008, both the large-scale circulation and episodic extremes appear to have contributed to the record rainfall totals.

In contrast to 2008, seasonal changes in Pacific sea surface temperatures toward moderate El Niño conditions by summertime appeared to have had a significant impact on the 2009 NAM (Fig. 11d). While the onset of the 2009 NAM was over a week early compared to climatology, the overall monsoon circulation pattern and its associated rainfall deteriorated substantially by late July. Consequently, July–August OLR anomalies (Fig. 11b) were mostly positive over the southwestern United States and Mexico. A number of areas of Mexico experienced some of the worst seasonal drought in recent history. Similarly, parts of western Arizona and the broader regions of the lower Colorado River valley experienced rainfall totals approaching only 50% of normal. Previous studies, cited above, have shown that El Niño conditions can suppress NAM rainfall, particularly over southern and eastern Mexico, by enhancing convection in the eastern Pacific ITCZ, reducing the northward transport of moisture and contributing to a poorly developed monsoon ridge structure, evidenced by the 200-mb height anomalies in Fig. 11f and a weakened overall monsoon circulation (Cavazos and Hastenrath 1990; Gochis et al. 2007). Related to this weaker-than-normal circulation pattern was a less-than-normal occurrence of tropical storm landfall and near-shore activity in both eastern and western NAM regions during 2009 (Fig. 7). The strong evolution in large-scale SST forcing and associated tropical activity during the YOTC appears to have had a significant impact on the timing (onset), intensity, and total accumulation of North American monsoon rainfall. However, seasonal forecasts had difficulty in both years predicting such impacts, highlighting the need for continued work in understanding large-scale ocean–monsoon interactions in North America.

South American. The South American monsoon (SAM) region extends from southern Amazonia and the upper Parana basin, and various studies have identified its characteristics and variability in various time scales (Ramage 1971; Zhou and Lau 1998; Vera et al. 2006; Liebmann et al. 2007; Marengo et al. 2012b). The "mature" phase of the monsoon in the SAM region occurs during the warm season, December–February, with the onset of the rainy season between September–November and the demise occurring after May [see Marengo et al. (2012b), and references therein]. The climatological onset of the SAM ranges between mid-October to early November, depending on the definition (Liebmann and Marengo 2001; Carvalho et al. 2011; Nieto-Ferreira and Rickenbach 2011), with the mean demise occuring in early May, and with both the onset and demise dates exhibiting interannual variability. Key variability influencing the onset and demise, as well as the strength and evolution of the SAM, are the South Atlantic convergence zone (SACZ) and the South America low-level jet (SALLJ) east of the Andes. Variations in the former have been found on intraseasonal-to-interdecadal time scales (Nogues-Paegle and Mo 1997; Grimm and Zilli 2009; Grimm 2010), and they often exhibit a dipole structure in rainfall between the SACZ and the subtopical plains just to the south. A strengthening of the SALLJ typically accompanies the suppressed SACZ–wet subtropical plains phase of the dipole, which transports massive amounts of moisture from the Amazon basin into the subtropics (Silva and Berbery 2006). In addition, strong SALLJ events are linked to short-term extreme precipitation events in the plains of central Argentina (Liebmann et al. 2004; Salio et al. 2007). In contrast, a SACZ-enhanced phase induces extreme heat waves over the subtropical regions (Cerne and Vera 2011).

For the YOTC period, rainfall in the September–November 2008 onset phase was below average over central-southern Brazil and most of Argentina (deficit exceeding 200 mm), with above-normal rainfall over the northern Amazon basin and portions of southern Brazil (Fig. 12a). In the mature phase, December 2008–February 2009 (Fig. 12b), rainfall was below average over the SAM region and in southern Brazil and most of Argentina, with anomalies greater than 270 mm. Above-average rainfall was observed over the northern Amazon basin and Northeast Brazil, with anomalies larger than 200 mm. During the decay phase, March–May 2009, well above-average rainfall was observed over northeastern Brazil and northern Amazonia (Fig. 12c). This is attributed to the anomalously warm tropical South Atlantic Ocean and a southward position of the ITCZ that usually moves northward in April but stayed in place until May. This resulted in anomalously strong moisture transport from the tropical Atlantic into the Amazon region. At this same time, La Niña conditions were evident in the tropical Pacific, which typically intensify the upward branches of the Walker and Hadley cells over Amazonia, and lead to abundant precipitation conditions. As a consequence of the intense rainfall, the Amazon basin exhibited heavy flooding, with water levels higher than in several decades. In July 2009, the

levels of the Rio Negro in Manaus reached 29.75 m, a new record high since the beginning of data collection in 1903. This resulted in over 300,000 people left homeless and 40 fatalities because of the floods (Marengo et al. 2012a). Another factor contributing to the intense rainfall in Northeast Brazil during this season was the active MJO (see Fig. 3; note the active MJO in the Eastern Hemisphere; the wide latitude averaging cancels out the signal in this diagram over South America).

For the 2009/10 monsoon season, warm SST conditions prevailed in the Pacific. During the onset season (Fig. 12d), negative rainfall anomalies were widespread, with dryer conditions persisting from northern Amazonia to Venezuela. This is attributed to an anomalous northward displacement of the ITCZ induced by warm surface waters in the tropical North Atlantic. Above-average rainfall was observed over parts of southern Brazil (about 280 mm above normal) and Paraguay, in association with increased frontal activity. During the mature phase, December 2009–February 2010 (Fig. 12e), rainfall totals were near average over the southern Amazon basin, and slightly below average over central Brazil and the north-central Amazon basin. Above-average rainfall was observed over southern Brazil, northeastern Argentina, Uruguay, and extreme northeastern Argentina, while below-average rainfall was observed over most of eastern Brazil. During March and April (Fig. 12f), rainfall totals were below average over central Brazil and Northeast Brazil and above average over Northeast Brazil. During this period, equatorial SSTs were 0.5°– 1°C above average across the eastern Pacific and 0.5°–1.5°C above average in the equatorial Atlantic, west of 10°W. This facilitated a northward migration of the ITCZ with dry conditions in Northeast Brazil and tropical South America east of the Andes, leading to one of the most intense droughts in Amazonia during the last 107 years (Marengo et al. 2011).

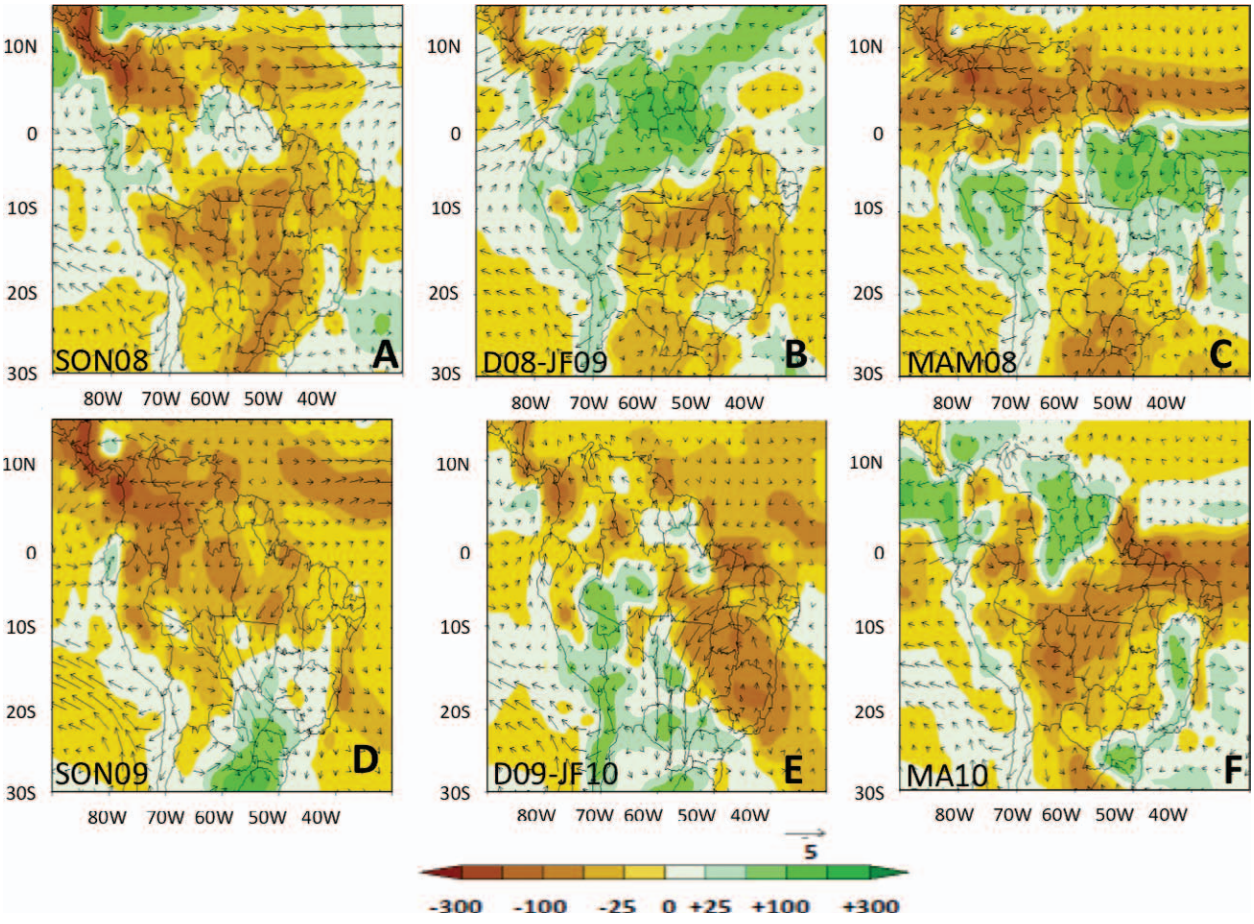

Fig. 12. Rainfall and 850-hPa winds for the SAM system. Arrows indicating wind scale (m s^{-1}) and color scale (mm) are shown at the bottom of the panel. (a) Sep–Nov 2008, (b) Dec 2008–Feb 2009, (c) Mar–May 2009, (d) Sep–Nov 2009, (e) Dec 2009–Feb 2010, and (f) Mar–Apr 2010. (Sources: CPTEC/INPE, São Paulo, Brazil, and NOAA/NCEP/CPC Maryland.)

West Africa. The year-to-year variability of Sahel rainfall, and thus the West African monsoon, is of great interest due to the very strong north–south gradient in natural and anthropogenic conditions. Figure 13 shows that both 2008 and 2009 May–September seasons were slightly wetter than the long-term average, consistent with a recent wet trend in this region (Fink et al. 2010). Further scrutiny illustrates that the anomalously wet Sahel signal in both years was mainly exhibited in the western Sahel west of about 0°E. The wet west Sahel in 2008 was part of a regional-scale wet anomaly that covered most of the West African region down to the Guinea coast. Other notable anomalies in 2008 included a drier (wetter)-than-normal Sudan (Ethiopian highlands). While the west Sahel was also wet in 2009, the West African region as a whole was drier compared to climatology, with notable dry anomalies in Liberia and the Ivory Coast, in much of Nigeria, and most prominently (compared to 2008) in the Sudan and Chad regions. The more widespread dry anomalies seen in 2009 compared to 2008 are consistent with the developing El Niño (Fig. 1). In addition, the relatively dry Guinea coast and wet Sahel would classify the 2009 season as a "dipole year" (Ward 1998), which is consistent with the observed cooler equatorial Atlantic during summer 2009 compared to 2008 (Fig. 1)

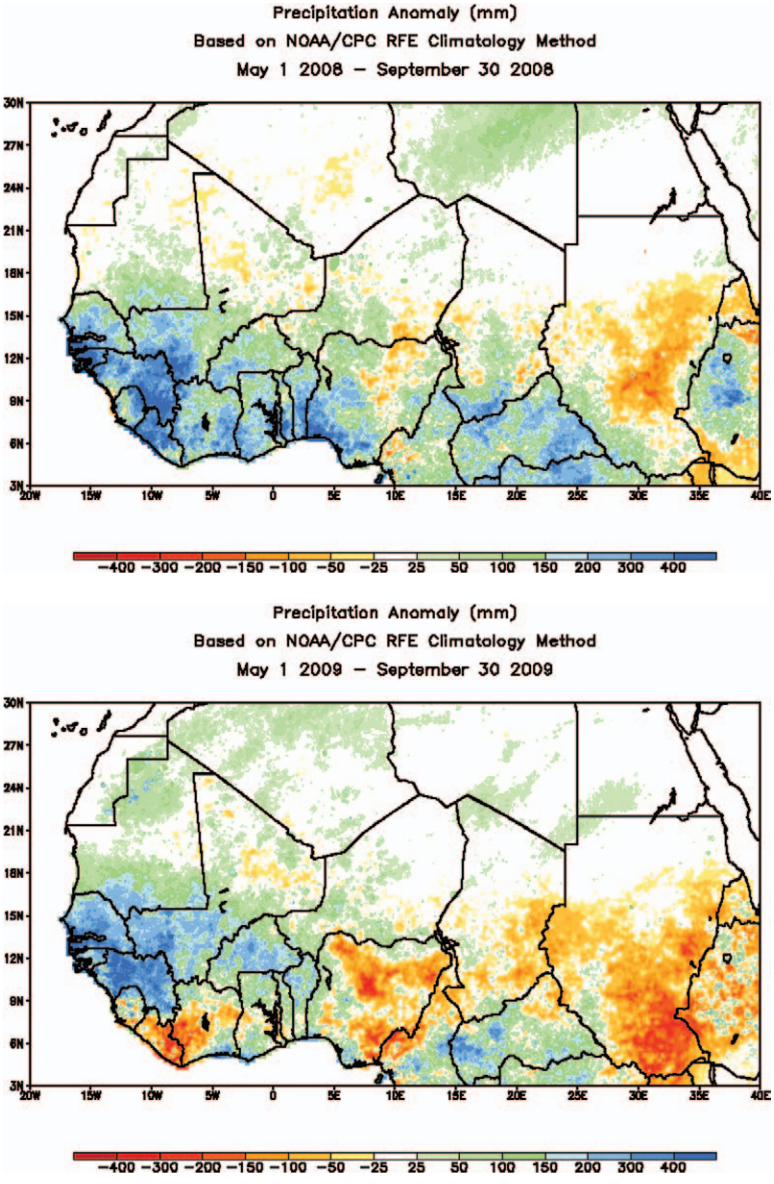

Fig. 13. Seasonal precipitation anomalies (mm) for 2008 and 2009 based on May–Sep rainfall totals and with reference to a climatology based on the years 1995–2001. Precipitation is estimated using the NOAA/CPC rainfall estimate (RFE) climatology method (see www.cpc.noaa.gov/products/fews/AFR_CLIM/afr_clim_season.shtml for more details).

West African monsoon onset and within-season rainfall variability, including their predictability, have received particular attention in recent years due to their obvious societal impacts (e.g., Sultan and Janicot 2000). The YOTC dataset should be exploited to establish the extent to which these can be understood and explained in terms of dynamical processes, such as inertial instability (e.g., Sultan and Janicot 2003; Hagos and Cook 2007; Nicholson and Webster 2007) or thermodynamic processes associated with variations in the Atlantic cold tongue (e.g., Okumura and Xie 2004), the Saharan heat low (e.g., Ramel et al. 2006), influences by ISV, including the MJO (Janicot et al. 2008; Barlow 2011), and the passage of CCEWs. An important component of West African monsoon variability is the presence of well-defined synoptic EWs, which account for 25%–35% of the total variance of deep convection (e.g., Mekonnen et al. 2006). This suggests a need to improve our understanding of the two-way interactions between the EWs (see "Easterly Waves" section) and the regional environment to better understand variability in the monsoon as well as the downstream

tropical Atlantic. Comparing Figs. 5 and 13 highlights the fact that the 2008 season was characterized by more EW activity and was generally wetter than in 2009, suggesting a potential relationship between the EW activity and seasonal rainfall. Studies indicate that EW activity can be influenced by rainfall modulation in the EWs themselves (Hsieh and Cook 2005, 2007), stability of the African easterly jet (e.g., Leroux and Hall 2009), triggering by tropical convection (e.g., Thorncroft et al. 2008; Leroux et al. 2010), and triggering by extratropical troughs (Leroux et al. 2011). The YOTC dataset should be exploited to ascertain the relative roles of these factors. Finally, it is now well known that Kelvin waves can significantly modulate rainfall and can both trigger and intensify EWs (e.g., Mekonnen et al. 2008; Ventrice et al. 2011). Figure 4 highlights the presence of Kelvin waves in spring, when they are known to be important in the equatorial African region (Nguyen and Duvel 2008), but they are also known to influence the Guinea coastal region of West Africa (not shown). Two notably strong Kelvin wave events occurred in early May 2008 and should be strong candidates for study in the YOTC dataset.

TROPICAL–EXTRATROPICAL INTERACTIONS. *Extratropical transition of tropical cyclones.* During extratropical transition (ET), tropical cyclones undergo significant structural changes, especially with regard to the distribution of deep convection, clouds, and precipitation (Jones et al. 2003). The interaction with the midlatitude flow during ET can lead to the excitation of a Rossby wave train (Harr and Dea 2009) and thus impact the midlatitude weather and predictability far from the location of the ET event (Anwender et al. 2008; Harr et al. 2008) (see also M12). A primary objective of T-PARC, which took place during the YOTC period, was to increase understanding of the impact of tropical cyclone structure on the ET process and subsequent midlatitude downstream development.

A unique set of observations of the structural changes during the ET of Typhoon Sinlaku (2008) was obtained during T-PARC. Following recurvature, Sinlaku was significantly altered by strong vertical wind shear from the west. The vortex core was tilted toward the east and the low-level circulation center was fully exposed as deep convection was suppressed. As the decaying Sinlaku approached southern Japan, several episodes of deep convection erupted to the east and downshear of the circulation center. The tropical cyclone reintensified to typhoon strength with a circulation center collocated with new episodes of the deep convection. In situ measurements obtained by T-PARC documented how the characteristic monopole vorticity structure evolved to a low-level center associated with the original tropical cyclone and a new vorticity center to the northeast, located in the region of the episodes of deep convection. Analysis of convective and stratiform precipitation from YOTC ECMWF analyses defined the presence of both cloud types in the region of the new vorticity maximum. Therefore, the diabatic fields indicate a tropical mesoscale circulation system with a stratiform region downstream from a leading convective cell. The reintensification period resulted in a stronger intensity and modified structure of Sinlaku as it eventually underwent ET, and thus it had an impact on its interaction with the midlatitude flow. During and following the ET, a small-scale Rossby wave train developed and appeared to interact with a larger-scale midlatitude Rossby wave train (Fig. 14c) No Rossby wave train is seen downstream of the second T-PARC ET case, Typhoon Jangmi. However, the divergent outflow from Jangmi appeared to accelerate a midlatitude jet streak.

During the YOTC period, low predictability, identified as increased standard deviation in the 3-, 5-, and 7-day forecasts of the ECMWF Ensemble Prediction System (EPS), is particularly marked when a clearly defined Rossby wave train develops or amplifies directly downstream of an ET event. This is seen for the ET of Halong in May 2008 (Figs. 14a,b), Bavi in October 2008 (Fig. 14c) and a further seven examples in the western North Pacific, two in the North Atlantic, and three in the Southern Hemisphere. In contrast, following the ET of Rammasun (Figs. 14a,b), ridging occurs downstream of the ET, but the Rossby wave train does not amplify until it reaches the eastern North Pacific. The EPS spread also increases at this stage. Similar behavior was seen in two other cases during the YOTC period. For Nakri in 2008 (Figs. 14a,b) and five Southern Hemisphere ETs, the main signal is a midlatitude Rossby wave train that is not modified during ET and exhibits weak-to-moderate EPS spread.

The YOTC period offers cases both of structural changes during ET as well as a variety of interactions between ET systems and the midlatitude flow. A priority for research with the combination of YOTC datasets and T-PARC observations will be to quantify the role of structural changes of the tropical cyclone before and during ET (e.g., increased outflow at upper levels, increased heat and moisture transport to midlatitudes) on the downstream midlatitude predictability (see M12).

Extratropical influences on the tropics. Upper-level disturbances penetrating from the extratropics into the subtropics and outer tropics can significantly influence the weather (e.g., Knippertz 2007, and references therein) and wave activity in the tropical belt, including Kelvin waves (e.g., Straub and Kiladis 2003), mixed Rossby–gravity waves (e.g., Magaña and Yanai 1995) and the MJO (e.g., Weickmann et al. 1985; see review by Roundy 2011). The eastern tropical Atlantic and Pacific Oceans and the adjacent landmasses are frequently affected by such tropical–extratropical interactions. As an example, we focus on West Africa, where upper-level disturbances regularly trigger moderate precipitation events during the boreal winter dry season (Knippertz and Fink 2008, 2009]. These significant anomalies can lead to high impacts on the affected population (e.g., rotting harvests, improved mango yield and grazing conditions, locusts). In extreme cases, heavy precipitation, flooding, destruction of infrastructure, and loss of lives can occur (Knippertz and Martin 2005; Meier and Knippertz 2009).

During the two dry seasons of the YOTC period, five significant West African wet episodes occurred: 5–6 December 2008, 8–9 January 2009, 16–19 February 2009, 31 October–1 November 2009, and 12–14 December 2009. Here, we will briefly discuss the February 2009 case as an illustration of the phenomenon (Knippertz and Fink 2008, 2009). Figure 15a shows accumulated precipitation from over the 4-day February 2009 period. Heavy precipitation occurred over northern Ivory Coast, southeastern Guinea, and southern Mali, with light precipitation extending across the Sahel far into the southern Sahara. These rainfalls were preceded by a wave-breaking event over the North Atlantic that generated a trough with a strongly positive tilt in the horizontal over Morocco and Algeria on 16 February 2009 (marked in figure). Tight gradients in the geopotential at 300 hPa all across northern Africa indicate a subtropical jet streak. The mean sea level pressure (MSLP) falls significantly to the southeast of the trough (i.e., in the right entrance region of the jet streak), leading to a northward shift of the weak wintertime heat low to eastern Burkina Faso on 16 February 2009 ("X" in Fig. 15), 5° to the north of its climatological position. The associated enhanced north–south MSLP gradient at its equatorward flank allows moist air from the Gulf of Guinea to penetrate farther than usual into the continent and feed the rainfall. The upper trough drifts southwestward along the northwest African coast until 19 February while the surface low slowly weakens (not shown). The resulting rainfall is mainly related to rather short-lived cellular convection during the afternoon and evening of 16–18 February and a slightly more organized system in the early morning hours of 19 February. These systems occur at the southern end

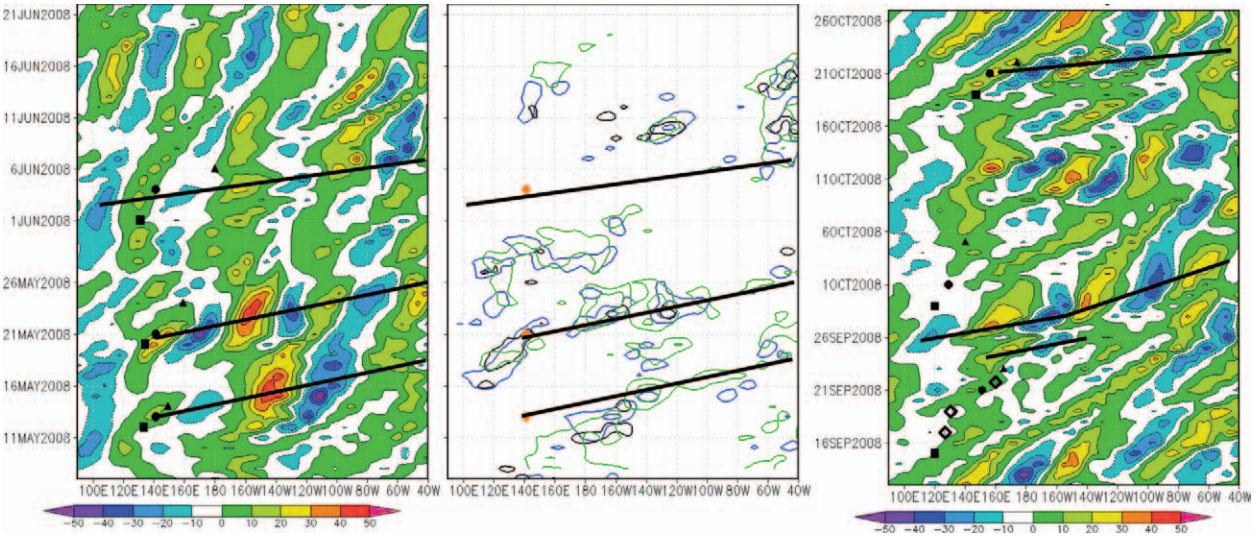

Fig. 14. Hovmöller plots across WNP of (left) 200-hPa meridional wind (m s^{-1}) from 6 May to 22 Jun 2008 averaged from 40° to 60°N, and (middle) 500-hPa height standard deviation from ECMWF EPS for 3-day forecast (black), 5-day forecast (blue), and 7-day forecast (green). (right) As in (left), but from 12 Sep to 27 Oct. Typhoon recurvature is marked on (left) and (right) by a black square, ET by a black circle, and decay point by a black triangle. The red circles on (middle) mark the ET time. Typhoons marked are (from top to bottom) Rammasun, Halong, and Nakri in (left) and (right) and Sinlaku, Jangmi, and Bavi in (right). [Figure courtesy of Julia Keller. Data taken from the ECMWF YOTC analyses and the THORPEX Interactive Grand Global Ensemble (TIGGE) database.]

of an extended southwest–northeast-oriented cloud band [a so-called "tropical plume"; see Knippertz (2007)] that drifts very slowly westward during 16–20 February in connection with the movement of the upper trough (Fig. 15c). A vertical cross section through this plume showing *CloudSat* radar reflectivity (Fig. 15d) indicates a sudden south–north decrease in cloud-top height and three bands of precipitation Strong evaporation at low levels, however, inhibits significant accumulations (Fig. 15a).

Consistent with results by Knippertz and Fink (2009), the general northward shift of the rain zone was reasonably well predicted with 5-day leads by the ECMWF. Despite this, the relative contributions of dynamical-versus-diabatic processes to the pressure fall are not well understood (Knippertz and Fink 2008), and details of the associated moisture inflow from the Gulf of Guinea and the ensuing tropical convection challenge present-day forecast models. Note the synergistic use of the high-resolution ECMWF YOTC analyses, station measurements, and satellite data to develop a robust characterization of this multifaceted and impactful event—a capability that YOTC objectives are focused on facilitating (see M12).

Atmospheric rivers. Atmospheric rivers (ARs) are narrow channels of enhanced atmospheric moisture transport that play a key role in the tropical–extratropical water cycle. Occupying ~10% of the Earth's circumference in the midlatitudes, they account for over 90% of the poleward moisture transport (Zhu and Newell 1994, 1998). They largely form in the extratropical ocean basins north of the tropical moisture reservoir. Some ARs are more directly

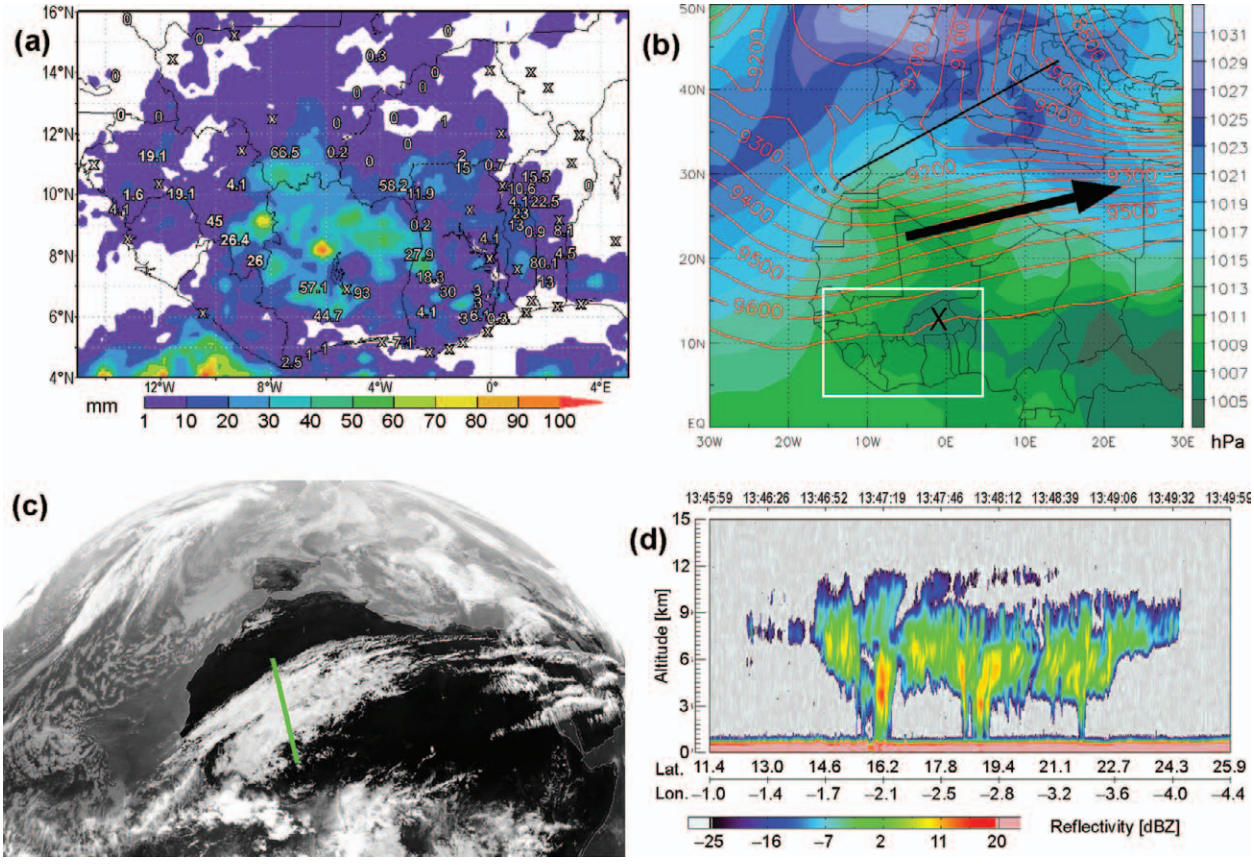

Fig. 15. An unusual dry-season rainfall event in tropical West Africa during 16–20 Feb 2009. (a) Precipitation accumulated over the 4-day period 0600 UTC 16 Feb–0600 UTC 20 Feb 2009 from the TRMM 3B42 3-hourly rainfall product (colors) and from surface rain gauges (numbers); values in mm. Symbol "x" stands for "no precipitation" and "0" stands for "traces of precipitation." Some stations have gaps in their records and therefore amounts must be considered as lower bounds. (b) Geopotential height at 300 hPa (contours every 50 gpm) and MSLP (hPa; colors) for 1200 UTC 16 Feb 2009. Data are taken from the ECMWF YOTC analysis. The upper-trough axis, the subtropical jet streak, and the pressure minimum over Burkina Faso are indicated. The area shown in (a) is bordered by a white box. (c) Meteosat channel 9 (infrared; 10.8 μm) at 1200 UTC 19 Feb 2009. (d) Vertical profile of reflectivity (dBz) from the *CloudSat* cloud-profiling radar along the green line shown in (c) between 1346 and 1350 UTC 19 Feb 2009.

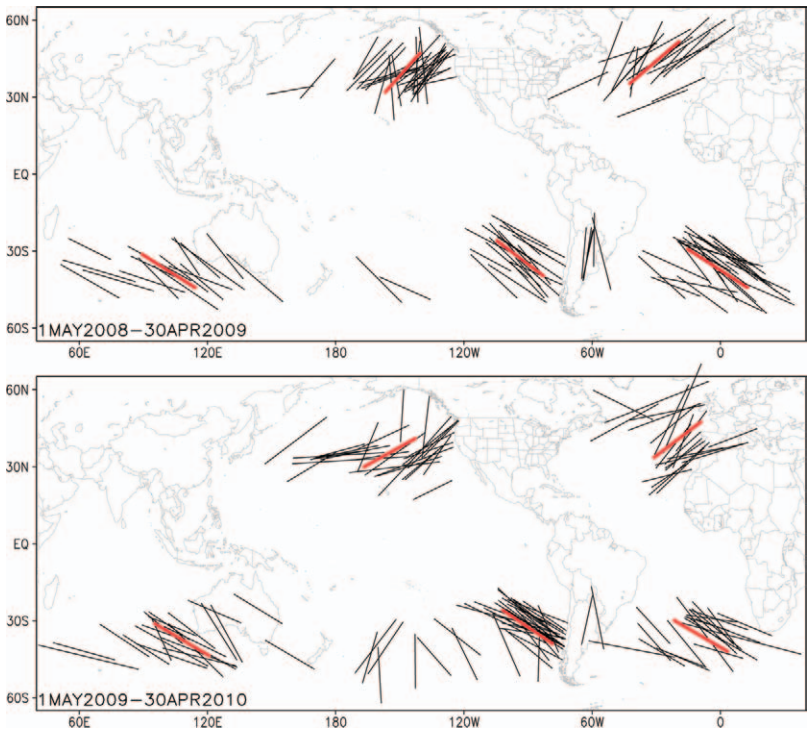

Fig. 16. Approximate locations (main axes; black lines) of ARs during the YOTC period. Red lines indicate the mean locations of the ARs within each ocean basin (the few isolated ARs west of 120°W were not included in the calculation for the southeastern Pacific). ARs are identified as long (>2,000 km), narrow (<1,000 km) plumes of enhanced (>2 cm) IWV in the daily maps observed by the AIRS instrument, following the criteria set in Ralph et al. (2004). The AIRS version 5 level 3 standard retrievals are used, which are globally available on a 1° × 1° grid. Daily means are first formed by weighting the ascending and descending satellite passes with the number of data counts within each grid cell. (top) 1 May 2008–30 Apr 2009. (bottom) 1 May 2009–30 Apr 2010.

linked to the tropics with moisture supplied by the tropical plumes, while some ARs show more of a subtropical or midlatitude moisture source (e.g., Ryoo et al. 2011). Landfalling ARs often lead to enhanced precipitation in the mountains of the west coast of North America, and are responsible for some extreme precipitation/flood events in the region (Ralph et al. 2006; Neiman et al. 2008a). Detection of ARs involves identifying narrow channels of enhanced moisture, typically identified in satellite observations of integrated water vapor (IWV) (Ralph et al. 2004; Neiman et al. 2008b). For this overview of the ARs during YOTC, daily maps of IWV from the Atmospheric Infrared Sounder (AIRS) were manually examined for AR-like structures (i.e., moisture plumes with 2 cm or greater IWV, narrower than 1,000 km, and longer than about 2,000 km; Ralph et al. 2004). Approximate locations of the ARs identified are shown in Fig. 16 for the two half periods (i.e. years) of YOTC.[1] A total of 259 ARs are identified, with 122 and 137 during the first and second half periods, respectively. In the first year, the maximum number of ARs occurred in the northeastern Pacific, with a similar number observed there in the second year. The southeastern Pacific, in contrast, saw an increase of 70% in the number of ARs in the second year. This is likely to be an influence of ENSO but the manner in which this may be so has not been established. Noteworthy is the scarcity of landfalling ARs in California during the YOTC period, as the average occurrence is about 15 per year (Neiman et al. 2008b). It is also worth noting that the tropical plume events/wet episodes over West Africa discussed in the previous subsection were not associated with ARs according to the IWV threshold

The impact of landfalling ARs is illustrated in Fig. 17 with an example of an extreme precipitation event in California's Sierra Nevada. There, a few Arkansas events can result in as large as 40% of the total seasonal snow accumulation (Guan et al. 2010)—an important water resource during summer. The figure shows the IWV plume and the 3-day cumulative precipitation associated with this event, which reached 9 cm on average.[2] A number of studies have showed the connection of the MJO to precipitation extremes in the U.S. West Coast and elsewhere (Mo and Higgins 1998b,a; Jones 2000; Bond and Vecchi

[1] AIRS data are not available during 10–25 January 2010 due to hardware failure. AR detection was not performed for that period.

[2] Three high-impact (3-day cumulative precipitation >9 cm in the Sierra Nevada) Arkansas events in California were identified during the YOTC period. However, none of them strictly conformed to the Ralph et al. (2011) criteria in terms of length or overall structure, including the one discussed here, which was 5% shorter than the criteria and thus is not included in Fig. 16. Three ARs meeting the criteria were identified in California during YOTC, but all with low impact (3-day cumulative precipitation <0.5 cm in the Sierra Nevada).

2003). Ralph et al. (2011) showed an interesting case in which the development of a high-impact Arkansas that made landfall over the Pacific Northwest was favored by MJO convection over the eastern Indian Ocean and equatorward Rossby wave energy propagation. Analysis of snow accumulation in the Sierra Nevada showed a preference of AR-related extreme events to occur when MJO activity is enhanced in the far western Pacific (Guan et al. 2010). Three AR-related extreme precipitation events during YOTC (including the one discussed here) occurred during relatively weak MJOs (amplitude ≤1) in the Indian/western Pacific Oceans. It remains to be explored and understood how conditions in the tropics (such as convection and circulation anomalies associated with MJO and ENSO) and tropical–extratropical interactions affect the formation and impact of ARs. The complexity of the multiscale interactions involved in such processes, as illustrated in Ralph et al. (2011), is of crucial interest to YOTC

SUMMARY. The discussion above highlights the diverse and impactful nature of the weather and climate associated with the WCRP–WWRP/THORPEX YOTC period of interest. Notable is the wide range of scale interactions involving tropical convection, particularly in terms of how the influence of ENSO cascades across a number of time scales and phenomena, including significant impacts on most of the monsoon circulations discussed, the nature of the intraseasonal variability, the structure and intensity of easterly waves, as well as the spatial modulation of extreme events, such as tropical cyclones and atmospheric rivers. Significant highlights, apart from the cool to warm transition in ENSO, are the severe drought monsoon for India in 2009 and the near-record setting North American monsoon in 2008. There was a fantastic tropical wave event in 2008 that impacted variability from the Indian to the Pacific/America sectors and extreme events in both the Western and Eastern Hemispheres, and other examples of convectively coupled wave–wave interactions. There were high-impact rainfall events in Africa that derived from tropical sources (i.e. easterly waves) in both 2008 and 2009 and a number of cases that arose from the influence of the extratropics. The tropical cyclone activity during YOTC, while being exceptionally quiet relative to the last 30 years, exhibited numerous highlights, including Ike—one of the largest storms ever recorded in aerial size in the Atlantic; Nargis—which led to disastrous consequences in Myanmar, three hurricanes making landfall onto Mexico from the Pacific in 2008, the 1.8 m of rainfall over the Philippines from slow-moving Typhoon Parma; Rick—the second strongest hurricane on record in the Pacific; high-latitude Hurricane Grace tracking across the United Kingdom; and a highly unusual South Atlantic storm named Anita. Moreover, the impact of ETs on the midlatitude flow during the entire YOTC period exhibits substantial variability both in terms of the excitation of Rossby wave trains and the predictive skill of this process. The objectives of YOTC are to highlight these types of features and phenomena and promote their interrogation via theory, observations, and models so that improved understanding and predictions can be afforded.

With the backing of the World Climate Research Programme and the World Weather Research Programme/THORPEX, the YOTC research program

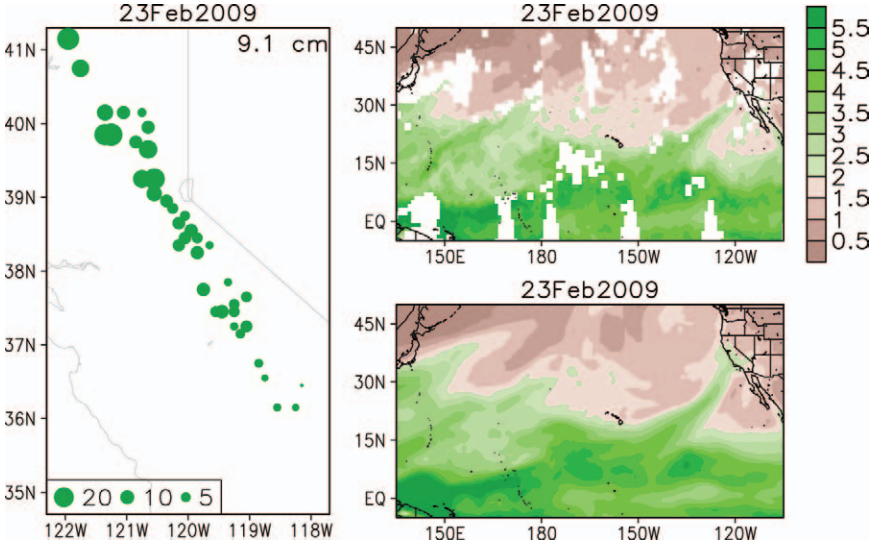

Fig. 17. An AR event on 23 Feb 2009. (left) Three-day cumulative precipitation (cm; centered on the Arkansas date) observed at snow sensor sites across the Sierra Nevada. Data were obtained from the California Department of Water Resources (http://cdec.water.ca.gov/). Domain-averaged precipitation is indicated in the top-right corner of the panel. (right) Daily mean IWV (cm) from (top right) the AIRS instrument and (bottom right) the ECMWF YOTC dataset.

is developing a suite of state-of-the-art datasets to examine the aforementioned weather and climate highlights in more detail. These include high-resolution atmospheric analyses from ECMWF, the National Centers for Environmental Prediction (NCEP), and the National Aeronautics and

SHALLOW CONVECTION PROCESSES: A VOCALS AND YOTC OVERLAP

Understanding shallow convection processes is critical to achieving better simulations and predictions associated with the expansive, low-level, high-albedo cloud regions of the tropics as well as transitions between shallow and deep convection. A primary goal of the VOCALS Regional Experiment (REx) is to characterize the structural properties of the marine boundary layer (MBL) over the southeastern tropical Pacific. In particular, components of the VOCALS field campaign were designed to better characterize the dominant forms of mesoscale cellular convection (MCC), which in the southeastern tropical Pacific includes closed cell and open cell structures, the latter with broken cloud and lower albedo. Pockets of open cells (POC) usually form within overcast closed MCC (Bretherton et al. 2004; Stevens et al. 2005; Comstock et al. 2007; Wood et al. 2008). The transition from closed to open cells represents a shift from a system driven primarily by cloud-top longwave cooling to a more cumuliform structure in which lifting is in part forced at the surface by localized cold pools formed by the evaporation of drizzle (Wang and Feingold 2009; Feingold et al. 2010).

The intensive observational phase of VOCALS-REx took place during October and November 2008 and involved five aircraft, two ships, and several ground sites (Wood et al. 2010a,b). Satellite imagery of the 27/28 October 2008 POC event (Fig. SB1a) shows the formation of a POC aligned roughly NW–SE within overcast stratocumulus clouds early in the morning of 27 October Ship radar observations (Fig. 1b sidebar) reveal locally intense drizzle cells surrounded by drizzle-free regions. The aircraft observations on the Nebraska side sampled during the evening of 27 October and early morning of 28 October reveal marked transitions in drizzle structure, and in cloud and aerosol microphysical properties across the boundary (Wood et al. 2010a). Ship radar observations in the overcast region to the southwest of the POC revealed the presence of more diffuse drizzling cells (Fig. SB1c) that have peak rain rates less than the echoes observed within the POC. Subsequently, the POC evolved by growing in width and advecting to the northwest with the synoptic flow. The VOCALS-REx dataset and the complementary elements of the YOTC project (see companion article M12) provide promising avenues for improving our basic understanding of these processes, including capturing their bulk effects in our global weather and climate models.

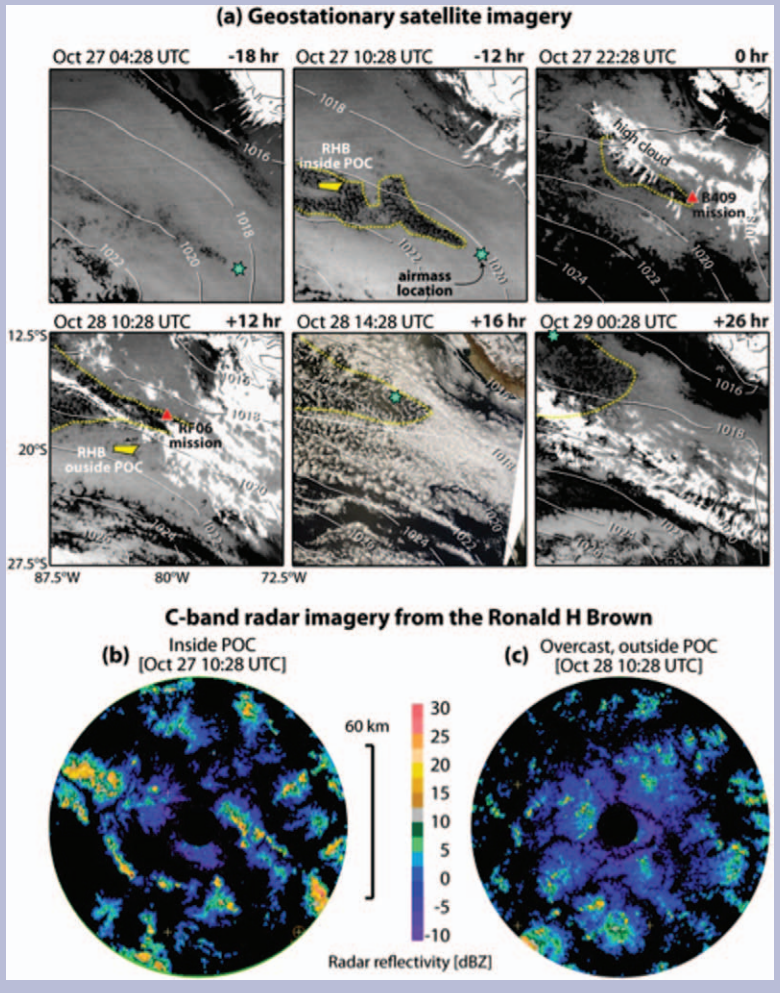

Fig. SB1. (a) Thermal infrared and visible (1428 UTC 28 Oct only) imagery for a 44-h period encompassing the intensive measurement period in which a POC is sampled by two aircraft (FAAM BAe-146 mission B409 and NSF/NCAR C-130 mission RF06) and the NOAA R/V *Ronald H. Brown (RHB)*. The POC is delineated by the dashed yellow line. The blue star shows the location along a 925-hPa trajectory of an air parcel initiated at the location/time shown in the top-left panel. These locations are indicated by red triangles for the images when the aircraft were sampling. (b),(c) Images of radar reflectivity from the C-band radar on the *RHB* for periods when the ship was inside the POC [for (b) see top-middle satellite image for ship location] and outside the POC [for (c), see bottom-left satellite image for ship location].

Space Administration (NASA), and a number of satellite data products, including a multisensor collocated dataset based on the Earth Observing System A-Train. Moreover, the YOTC period occurred in conjunction with the T-PARC and the Variability of the American Monsoon System (VAMOS) Ocean–Cloud–Atmosphere–Land Study (VOCALS) field programs as well as a multitude of activities associated with the Asian Monsoon Year (AMY), all of which allow additional resources and focus to be brought to bear on interrelated tropical convection issues. By leveraging these activities and resources, the YOTC Implementation Plan sets a course to develop a number of programmatic research activities, model studies, and intercomparisons. One particular focus is on using models in hindcast mode to explore their sensitivities and shortcomings in conjunction with the above observation resources to drive at improvements in our forecast capabilities from short-term to seasonal prediction. This program and its focus provide an initial framework to develop the techniques and know-how to approach the next generation of high-resolution models [e.g., global cloud-system-resolving models (CSRMs), multiscale modeling framework (MMF), regional and adaptive grid systems] that at present tax our abilities to fully exploit all our resources—both in terms of technical (e.g., network and analysis bandwidth) and scientific (multiscale interactions, multisensor constraints/evaluation) challenges. In this regard, YOTC provides an excellent and rich activity through which to entrain and train the next generation of weather, climate, and Earth scientists through graduate and postdoctoral research programs along with YOTC-related meetings and symposia.[3] This new generation will be ideally situated to capitalize on the new capabilities that have and are being put into place, including the interdisciplinary education and landscape being established to tackle the pressing environmental and societally impactful challenges associated with tropical convection. Focused period field programs, with YOTC representing a global virtual field program, represent key resources for the training scientists for many years to decades after their initial data acquisition (e.g., www.ametsoc.org/sloan/gate/). For additional motivation, scientific underpinnings and hypotheses associated with YOTC, see M12.

[3] Past activities include YOTC-sponsored sessions at six American Geophysical Union meetings, a session at an American Meteorological Society annual meeting, the First YOTC International Science Symposium, and a workshop on intraseasonal variability and the monsoon (see www.ucar.edu/yotc/meetings.html).

ACKNOWLEDGMENTS. We would like to express our gratitude to the World Climate Research Programme, the World Weather Research Programme, and The Observing System Research and Prediction Experiment (THORPEX) for their joint support of the YOTC program. This research was supported by the National Science Foundation, Mesoscale Dynamic Meteorology Program, under Grant ATM-0639461, and the National Oceanic and Atmospheric Administration, Office of Global Programs, under Grant NA07OAR4310263. The European Centre for Medium-Range Weather Forecasts is acknowledged for providing the special ECMWF YOTC dataset. We thank Paul Ciesielski and Andy Newman for their assistance in the preparation of figures. The *CloudSat* and TRMM data were visualized with the Giovanni online data system, developed and maintained by the NASA GES DISC. The Meteosat image was downloaded from the webpage of the Dundee Satellite Receiving Station. We are grateful to the ECMWF for providing access to the YOTC analysis and forecast products, and to the French IRD and the National Weather Services of Benin, Guinea, and Ghana for providing rainfall data for February 2009. BNG thanks Neena Mani Joseph and Suhas E for their help in creating the Indian monsoon figures. YLS was supported by NOAA's Climate Program Office under Grant NA06OAR43100. DJG was supported by NOAA's Climate Program Office under Grant NA08OAR4310705.

REFERENCES

Ajayamohan, R. S., S. A. Rao, and T. Yamagata, 2008: Influence of Indian Ocean dipole on poleward propagation of boreal summer intraseasonal oscillations. *J. Climate,* **21,** 5437–5454.

——, ——, J.-J. Luo, and T. Yamagata, 2009: Influence of Indian Ocean dipole on boreal summer intraseasonal oscillations in a coupled general circulation model. *J. Geophys. Res.,* **114,** D06119, doi:10.1029/2008JD011096.

Ambaum, M. H. P., B. J. Hoskins, and D. B. Stephenson, 2001: Arctic Oscillation or North Atlantic Oscillation? *J. Climate,* **14,** 3495–3507.

Anwender, D., P. A. Harr, and S. C. Jones, 2008: Predictability associated with the downstream impacts of the extratropical transition of tropical cyclones: Case studies. *Mon. Wea. Rev.,* **136,** 3226–3247.

Barlow, M., 2011: Africa and west Asia. *Intraseasonal Variability in the Atmosphere-Ocean Climate System.* 2nd ed. W. K.-M. Lau and D. E. Waliser, Eds., Springer, 477–496.

Black, E., J. Slingo, and K. R. Sperber, 2003: An observational study of the relationship between excessively strong short rains in coastal East Africa and Indian Ocean SST. *Mon. Wea. Rev.,* **131,** 74–94.

Bond, N. A., and G. A. Vecchi, 2003: The influence of the Madden–Julian oscillation on precipitation in Oregon and Washington. *Wea. Forecasting,* **18,** 600–613.

Bretherton, C. S., and Coauthors, 2004: The EPIC 2001 stratocumulus study. *Bull. Amer. Meteor. Soc.,* **85,** 967–977.

Carton, J., and B. Huang, 1994: Warm events in the tropical Atlantic. *J. Phys. Oceanogr.,* **24,** 888–903.

Carvalho, L. M. V., C. Jones, A. E. Silva, and B. Liebmann, and P. L. Silva Dias, 2011: The South American monsoon system and the 1970s climate transition. *Int. J. Climatol.,* **31,** 1248–1256.

Castro, C. L., T. B. McKee, and R. A. Pielke, 2001: The relationship of the North American monsoon to tropical and North Pacific sea surface temperatures as revealed by observational analyses. *J. Climate,* **14,** 4449–4473.

Cavazos, T., and S. Hastenrath, 1990: Convection and rainfall over Mexico and their modulation by the Southern Oscillation. *Int. J. Climatology,* **10,** 377–386.

Cerne, S. B., and C. S. Vera, 2011: Influence of the intraseasonal variability on heat waves in subtropical South America. *Climate Dyn.,* **36,** 2265–2277, doi:10.1007/s00382-010-0812-4.

Comstock, K. K., S. E. Yuter, R. Wood, and C. S. Bretherton, 2007: The three-dimensional structure and kinematics of drizzling stratocumulus. *Mon. Wea. Rev.,* **135,** 3767–3784.

Deser, C., 2000: On the teleconnectivity of the "Arctic Oscillation." *Geophys. Res. Lett.,* **27,** 779–782.

Drosdowsky, W., 1996: Variability of the Australian summer monsoon at Darwin: 1957–1992. *J. Climate,* **9,** 85–96.

Enfield, D. B., and D. A. Mayer, 1997: Tropical Atlantic sea surface temperature variability and its relation to El Niño-Southern Oscillation. *J. Geophys. Res.,* **102** (C1), 929–945.

Englehart, P. J., and A. V. Douglas, 2001: The role of eastern North Pacific tropical storms in the rainfall climatology of western Mexico. *Int. J. Climatol.,* **21,** 1357–1370.

Feingold, G., I. Koren, H. Wang, H. Xue, and W. A. Brewer, 2010: Precipitation-generated oscillations in open cellular cloud fields. *Nature,* **466,** 849–852, doi:10.1038/nature09314.

Fink, A. H., J. M. Schrage, and S. Kothaus, 2010: On the potential causes of the nonstationary correlations between West African precipitation and Atlantic hurricane activity. *J. Climate,* **23,** 5437–5456.

Gadgil, S., 1981: Fluid dynamics of the monsoon. *Proc. Indian Acad. Sci. Eng. Sci.,* **4,** 295–314.

Giannini, A., M. A. Cane, and Y. Kushnir, 2001: Interdecadal changes in the ENSO teleconnection to the Caribbean region and the North Atlantic Oscillation. *J. Climate,* **14,** 2867–2879.

Gochis, D. J., L. Brito-Castillo, and W. J. Shuttleworth, 2007: Correlations between sea-surface temperatures and warm season streamflow in northwest Mexico. *Int. J. Climatol.,* **27,** 883–901.

——, S. W. Nesbitt, W. Yu, and S. F. Williams, 2009: Comparison of gauge-corrected versus non-gauge corrected satellite-based quantitative precipitation estimates during the 2004 NAME enhanced observing period. *Atmósfera,* **22,** 69–98.

Goswami, B. N., 2011: South Asian summer monsoon. *Intraseasonal Variability in the Atmosphere-Ocean Climate System.* 2nd ed. W. K.-M. Lau and D. E. Waliser, Eds., Springer, 21–72.

Grimm, A. M., 2010: Interannual climate variability in South America: Impacts on seasonal precipitation, extreme events, and possible effects of climate change. *Stochastic Environ. Res. Risk Assess.,* **25,** 537–554, doi:10.1007/s00477-00010-00420-00471.

——, and M. Zilli, 2009: Interannual variability and seasonal evolution of summer monsoon in South America. *J. Climate,* **22,** 2257–2275.

Guan, B., N. P. Molotch, D. E. Waliser, E. J. Fetzer, and P. J. Neiman, 2010: Extreme snowfall events linked to atmospheric rivers and surface air temperature via satellite measurements. *Geophys. Res. Lett.,* **37,** L20401, doi:10.1029/2010GL044696.

Hagos, S., and K. Cook, 2007: Dynamics of the West African monsoon jump. *J. Climate,* **20,** 5264–5284.

Harr, P. A., and J. M. Dea, 2009: Downstream development associated with the extratropical transition of tropical cyclones over the western North Pacific. *Mon. Wea. Rev.,* **137,** 1295–1319.

——, D. Anwender, and S. C. Jones, 2008: Predictability associated with the downstream impacts of the extratropical transition of tropical cyclones: Methodology and a case study of Typhoon Nabi (2005). *Mon. Wea. Rev.,* **136,** 3205–3225.

Hastenrath, S., 1987: On the prediction of India monsoon rainfall anomalies. *J. Climate Appl. Meteor.,* **26,** 847–857.

——, and L. Greischar, 2001: The North Atlantic Oscillation in the NCEP–NCAR reanalysis. *J. Climate,* **14,** 2404–2413.

Hendon, H. H., C. D. Zhang, and J. D. Glick, 1999: Interannual variation of the Madden–Julian oscillation during austral summer. *J. Climate,* **12,** 2538–2550.

——, M. C. Wheeler, and C. D. Zhang, 2007: Seasonal dependence of the MJO–ENSO relationship. *J. Climate,* **20,** 531–543.

Higgins, R. W., K. C. Mo, and Y. Yao, 1998: Interannual variability of the U.S. summer precipitation regime with emphasis on the southwestern monsoon. *J. Climate,* **11,** 2582–2606.

——, W. Shi, and C. Hain, 2004: Relationships between Gulf of California moisture surges and precipitation in the southwestern United States. *J. Climate,* **17,** 2983–2997.

Horel, J. D., and J. M. Wallace, 1981: Planetary-scale atmospheric phenomena associated with the Southern Oscillation. *Mon. Wea. Rev.,* **109,** 813–829.

——, and ——, 1982: Reply. *Mon. Wea. Rev.,* **110,** 1497–1497.

Hsieh, J. S., and K. H. Cook, 2005: Generation of African easterly wave disturbances: Relationship to the African easterly jet. *Mon. Wea. Rev.,* **133,** 1311–1327.

——, and ——, 2007: A study of the energetics of African easterly waves using a regional climate model. *J. Atmos. Sci.,* **64,** 421–440.

Hsu, P. C., C. H. Tsou, H. H. Hsu, and J. H. Chen, 2009: Eddy energy along the tropical storm track in association with ENSO. *J. Meteor. Soc. Japan,* **87,** 687–704.

Huffman, G. J., and Coauthors, 2007: The TRMM Multisatellite Precipitation Analysis (TMPA): Quasi-global, multiyear, combined-sensor precipitation estimates at fine scales. *J. Hydrometeor.,* **8,** 38–55.

Hurrell, J. W., 1996: Influence of variations in extratropical wintertime teleconnections on Northern Hemisphere temperature. *Geophys. Res. Lett.,* **23,** 665–668.

Janicot, S., and Coauthors, 2008: Large-scale overview of the summer monsoon over West Africa during the AMMA field experiment in 2006. *Ann. Geophys.,* **26,** 2569–2595.

Janiga, M. A., 2010: Easterly wave structural evolution over West Africa and the east Atlantic. *Proc. 29th Conf. on Hurricanes and Tropical Meteorology,* Tucson, AZ, Amer. Meteor. Soc., 5D.6. [Available online at http://ams.confex.com/ams/29Hurricanes/techprogram/paper_168967.htm.]

Jones, C., 2000: Occurrence of extreme precipitation events in California and relationships with the Madden–Julian oscillation. *J. Climate,* **13,** 3576–3587.

Jones, S. C., and Coauthors, 2003: The extratropical transition of tropical cyclones: Forecast challenges, current understanding, and future directions. *Wea. Forecasting,* **18,** 1052–1092.

Joseph, S., A. K. Sahai, and B. N. Goswami, 2010: Boreal summer intraseasonal oscillations and seasonal Indian monsoon prediction in DEMETER coupled models. *Climate Dyn.,* **35,** 651–667, doi:10.1007/s00382-009-0635-3.

Kessler, W. S., 2001: EOF representations of the Madden–Julian oscillation and its connection with ENSO. *J. Climate,* **14,** 3055–3061.

Kiladis, G. N., C. D. Thorncroft, and N. M. J. Hall, 2006: Three-dimensional structure and dynamics of African easterly waves. Part I: Observations. *J. Atmos. Sci.,* **63,** 2212–2230.

——, M. C. Wheeler, P. T. Haertel, K. H. Straub, and P. E. Roundy, 2009: Convectively coupled equatorial waves. *Rev. Geophys.,* **47,** RG2003, doi:10.1029/2008RG000266.

Knippertz, P., 2007: Tropical–extratropical interactions related to upper-level troughs at low latitudes. *Dyn. Atmos. Oceans,* **43,** 36–62.

——, and J. E. Martin, 2005: Tropical plumes and extreme precipitation in subtropical and tropical West Africa. *Quart. J. Roy. Meteor. Soc.,* **131,** 2337–2365.

——, and A. H. Fink, 2008: Dry-season precipitation in tropical West Africa and its relation to forcing from the extratropics. *Mon. Wea. Rev.,* **136,** 3579–3596.

——, and ——, 2009: Prediction of dry-season precipitation in tropical West Africa and its relation to forcing from the extratropics. *Wea. Forecasting,* **24,** 1064–1084.

Kumar, A., and M. P. Hoerling, 1998: Annual cycle of Pacific–North American seasonal predictability associated with different phases of ENSO. *J. Climate,* **11,** 3295–3308.

Lau, K.-M., and H. Lim, 1982: Thermally driven motions in an equatorial β-plane: Hadley and Walker circulations during the winter monsoon. *Mon. Wea. Rev.,* **110,** 336–353.

Lau, N.-C., and M. J. Nath, 2006: ENSO modulation of the interannual and intraseasonal variability of the East Asian monsoon—A model study. *J. Climate,* **19,** 4508–4530.

Lau, W. K.-M., 2005: El Niño Southern Oscillation connection. *Intraseasonal Variability in the Atmosphere-Ocean Climate System,* 2nd ed. W. K.-M. Lau and D. E. Waliser, Eds., Springer, 271–306.

——, and D. E. Waliser, Eds., 2011: *Intraseasonal Variability in the Atmosphere-Ocean Climate System*. 2nd ed. W. K.-M. Lau and D. E. Waliser, Eds., Springer, 1102 pp.

Leroux, S., and N. M. J. Hall, 2009: On the relationship between African easterly waves and the African easterly jet. *J. Atmos. Sci.,* **66,** 2303–2316.

——, ——, and G. N. Kiladis, 2010: A climatological study of transient–mean-flow interactions over West Africa. *Quart. J. Roy. Meteor. Soc.,* **136,** 397–410.

——, ——, ——, 2011: Intermittent African easterly wave activity in a dry atmospheric model: Influence of the extratropics. *J. Climate,* **24,** 5378–5396.

L'Heureux, M. L., and R. W. Higgins, 2008: Boreal winter links between the Madden–Julian oscillation and the Arctic Oscillation. *J. Climate,* **21,** 3040–3050.

Liebmann, B., and J. A. Marengo, 2001: Interannual variability of the rainy season and rainfall in the Brazilian Amazon basin. *J. Climate,* **14,** 4308–4318.

——, G. N. Kiladis, C. S. Vera, A. C. Saulo, and L. M. V. Carvalho, 2004: Subseasonal variations of rainfall in South America in the vicinity of the low-level jet east of the Andes and comparison to those in the South Atlantic convergence zone. *J. Climate,* **17,** 3829–3842.

——, S. J. Camargo, A. Seth, J. A. Marengo, L. M. V. Carvalho, D. Allured, R. Fu, and C. S. Vera, 2007: Onset and end of the rainy season in South America in observations and the ECHAM 4.5 atmospheric general circulation model. *J. Climate,* **20,** 2037–2050.

——, I. Blade, N. A. Bond, D. Gochis, D. Allured, and G. T. Bates, 2008: Characteristics of North American summertime rainfall with emphasis on the monsoon. *J. Climate,* **21,** 1277–1294.

Madden, R. A., and P. R. Julian, 1971: Detection of a 40–50 day oscillation in zonal wind in tropical pacific. *J. Atmos. Sci.,* **28,** 702–708.

Magaña, V., and M. Yanai, 1995: Mixed Rossby–gravity waves triggered by lateral forcing. *J. Atmos. Sci.,* **52,** 1473–1486.

Marengo, J. A., J. Tomasella, L. M. Alves, W. R. Soares, and D. A. Rodriguez, 2011: The drought of 2010 in the context of historical droughts in the Amazon region. *Geophys. Res. Lett.,* **38,** L12703, doi:10.1029/2011GL047436.

——, ——, W. R. Soares, L. M. Alves, and C. A. Nobre, 2012a: Extreme climatic events in the Amazon basin: Climatological and hydrological context of recent floods. *Theor. Appl. Climatol.,* **107,** 73–85, doi:10.1007/s00704-011-0465-1.

——, and Coauthors, 2012b: Recent developments on the South American monsoon system. *Int. J. Climatology,* **32,** 1–21.

Maue, R. N., 2009: Northern Hemisphere tropical cyclone activity. *Geophys. Res. Lett.,* **36,** L05805, doi:10.1029/2008GL035946.

——, 2011: Recent historically low global tropical cyclone activity. *Geophys. Res. Lett.,* **38,** L14803, doi: 10.1029/2011GL047711.

Meier, F., and P. Knippertz, 2009: Dynamics and predictability of a heavy dry-season precipitation event over West Africa—Sensitivity experiments with a global model. *Mon. Wea. Rev.,* **137,** 189–206.

Mekonnen, A., C. D. Thorncroft, and A. R. Aiyyer, 2006: Analysis of convection and its association with African easterly waves. *J. Climate,* **19,** 5405–5421.

——, ——, ——, and G. N. Kiladis, 2008: Convectively coupled Kelvin waves over tropical Africa during the boreal summer: Structure and variability. *J. Climate,* **21,** 6649–6667.

Mo, K. C., and R. W. Higgins, 1998a: Tropical convection and precipitation regimes in the western United States. *J. Climate,* **11,** 2404–2423.

——, and ——, 1998b: Tropical influences on California precipitation. *J. Climate,* **11,** 412–430.

Moncrieff, M. W., M. Shapiro, J. Slingo, and F. Molteni, 2007: Collaborative research at the intersection of weather and climate. *WMO Bull.,* **56,** 204–211.

——, D. E. Waliser, M. Miller, M. A. Shapiro, G. R. Asrar, and J. Caughey, 2012: Multiscale convective organization and the YOTC virtual global field campaign, *Bull. Amer. Meteor. Soc.,* **93,** 1171–1187.

Murakami, T., 1975: Temporal variation of monsoon circulation. *Bull. Amer. Meteor. Soc.,* **56,** 309–309.

Neena, J. M., E. Suhas, and B. N. Goswam, 2011: Leading role of internal dynamics in the 2009 Indian summer monsoon drought. *J. Geophys. Res.,* **116,** D13103, doi:10.1029/2010JD015328.

Neiman, P. J., F. M. Ralph, G. A. Wick, Y. H. Kuo, T. K. Wee, Z. Z. Ma, G. H. Taylor, and M. D. Dettinger, 2008a: Diagnosis of an intense atmospheric river impacting the Pacific Northwest: Storm summary and offshore vertical structure observed with COSMIC satellite retrievals. *Mon. Wea. Rev.,* **136,** 4398–4420.

——, ——, ——, J. D. Lundquist, and M. D. Dettinger, 2008b: Meteorological characteristics and overland precipitation impacts of atmospheric rivers affecting the west coast of North America based on eight years of SSM/I satellite observations. *J. Hydrometeor.,* **9,** 22–47.

Newman, M., and P. D. Sardeshmukh, 1998: The impact of the annual cycle on the North Pacific/North American response to remote low-frequency forcing. *J. Atmos. Sci.,* **55,** 1336–1353.

Nguyen, T. T. H., and J. P. Duvel, 2008: Synoptic wave perturbations and convective systems over equatorial Africa. *J. Climate,* **21,** 6372–6388.

Nicholls, N., J. L. McBride, and R. J. Ormerod, 1982: On predicting the onset of the Australian wet season at Darwin. *Mon. Wea. Rev.,* **110,** 14–17.

Nicholson, S. E., and P. J. Webster, 2007: A physical basis for the interannual variability of rainfall in the Sahel. *Quart. J. Roy. Meteor. Soc.,* **133,** 2065–2084.

Nieto-Ferreira, R., and T. M. Rickenbach, 2011: Regionality of monsoon onset in South America: A

three-stage conceptual model. *Int. J. Climatol.,* **31,** 1309–1321.

Nitta, T., and Y. Takayabu, 1985: Global analysis of the lower tropospheric disturbances in the tropics during the northern summer of the FGGE year. Part II: Regional characteristics of the disturbances. *Pure Appl. Geophys.,* **123,** 272–292.

Nogues-Paegle, J., and K. C. Mo, 1997: Alternating wet and dry conditions over South America during summer. *Mon. Wea. Rev.,* **125,** 279–291.

Okumura, Y., and S.-P. Xie, 2004: Interaction of the Atlantic equatorial cold tongue and the African monsoon. *J. Climate,* **17,** 3589–3602.

Ostermeier, G. M., and J. M. Wallace, 2003: Trends in the North Atlantic Oscillation–Northern Hemisphere annular mode during the twentieth century. *J. Climate,* **16,** 336–341.

Pohl, B., N. Fauchereau, C. J. C. Reason, and M. Rouault, 2010: Relationships between the Antarctic Oscillation, the Madden–Julian Oscillation, and ENSO, and consequences for rainfall analysis. *J. Climate,* **23,** 238–254.

Pope, M., C. Jakob, and M. J. Reeder, 2009: Regimes of the north Australian wet season. *J. Climate,* **22,** 6699–6715.

Ralph, F. M., P. J. Neiman, and G. A. Wick, 2004: Satellite and CALJET aircraft observations of atmospheric rivers over the eastern North Pacific Ocean during the winter of 1997/98. *Mon. Wea. Rev.,* **132,** 1721–1745.

——, ——, ——, S. I. Gutman, M. D. Dettinger, D. R. Cayan, and A. B. White, 2006: Flooding on California's Russian River: Role of atmospheric rivers. *Geophys. Res. Lett.,* **33,** L13801, doi:10.1029/2006GL026689.

——, ——, G. N. Kiladis, K. Weickmann, and D. W. Reynolds, 2011: A multiscale observational case study of a Pacific atmospheric river exhibiting tropical–extratropical connections and a mesoscale frontal wave. *Mon. Wea. Rev.,* **139,** 1169–1189.

Ramage, C. S., 1971: *Monsoon Meteorology.* International Geophysics Series, Vol. 15, Academic Press, 296 pp.

Ramel, R., H. Gallée, and C. Messager, 2006: On the northward shift of the West African monsoon. *Climate Dyn.,* **26,** 429–440.

Rao, S. A., S. Masson, J.-J. Luo, S. K. Behera, and T. Yamagata, 2007: Termination of Indian Ocean dipole events in a coupled general circulation model. *J. Climate,* **20,** 3018–3035.

Redelsperger, J.-L., C. D. Thorncroft, A. Diedhiou, T. Lebel, D. J. Parker, and J. Polcher, 2006: African Monsoon Multidisciplinary Analysis: An international research project and field campaign. *Bull. Amer. Meteor. Soc.,* **87,** 1739–1746.

Reed, R., and E. Recker, 1971: Structure and properties of synoptic-scale wave disturbances in the equatorial western Pacific. *J. Atmos. Sci.,* **28,** 1117–1133.

——, D. Norquist, and E. Recker, 1977: The structure and properties of African wave disturbances as observed during phase III of GATE. *Mon. Wea. Rev.,* **105,** 317–333.

Renwick, J. A., and J. M. Wallace, 1996: Relationships between North Pacific wintertime blocking, El Niño, and the PNA pattern. *Mon. Wea. Rev.,* **124,** 2071–2076.

Rodwell, M. J., and B. J. Hoskins, 2001: Subtropical anticyclones and summer monsoons. *J. Climate,* **14,** 3192–3211.

Roundy, P., 2011: Tropical–extratropical interactions. *Intraseasonal Variability in the Atmosphere-Ocean Climate System,* 2nd ed. W. K.-M. Lau and D. E. Waliser, Eds., Springer, 497–512.

Ryoo, J. M., D. Waliser, and E. Fetzer, 2011: Trajectory analysis on the origin of air mass and moisture associated with atmospheric rivers over the West Coast of the United States. *Atmos. Chem. Phys. Discuss.,* **11,** 11 109–11 142.

Saji, N. H., B. N. Goswami, P. N. Vinayachandran, and T. Yamagata, 1999: A dipole mode in the tropical Indian Ocean. *Nature,* **401,** 360–363.

Salio, P., M. Nicolini, and E. J. Zipser, 2007: Mesoscale convective systems over southeastern South America and their relationship with the South American low level jet. *Mon. Wea. Rev.,* **135,** 1290–1309.

Serra, Y. L., 2009: Easterly wave activity and its modulation by the larger scales during the YOTC time period of focus: May 2008–Oct 2009. *Eos, Trans. Amer. Geophys. Union,* **90** (Fall Meeting Suppl.), Abstract A41F-07.

——, G. N. Kiladis, and M. F. Cronin, 2008: Horizontal and vertical structure of easterly waves in the Pacific ITCZ. *J. Atmos. Sci.,* **65,** 1266–1284.

Silva, V. B. S., and E. H. Berbery, 2006: Intense rainfall events affecting the La Plata Basin. *J. Hydrometeor.,* **7,** 769–787.

Stevens, B., G. Vali, K. Comstock, R. Wood, M. C. Van Zanten, P. H. Austin, C. S. Bretherton, and D. H. Lenschow, 2005: Pockets of open cells and drizzle in marine stratocumulus. *Bull. Amer. Meteor. Soc.,* **86,** 51–57.

Straub, K. H., and G. N. Kiladis, 2003: Extratropical forcing of convectively coupled Kelvin waves during austral winter. *J. Atmos. Sci.,* **60,** 526–543.

Sultan, B., and S. Janicot, 2000: Abrupt shift of the ITCZ over West Africa and intra-seasonal variability. *Geophys. Res. Lett.,* **27,** 3353–3356.

——, and ——, 2003: The West African monsoon dynamics. Part II: The "preonset" and "onset" of the summer monsoon. *J. Climate,* **16,** 3407–3427.

Takayabu, Y. N., 1994: Large-scale cloud disturbances associated with equatorial waves. Part I: Spectral features of the cloud disturbances. *J. Meteor. Soc. Japan,* **72,** 433–449.

Thompson, D. W. J., and J. M. Wallace, 1998: The Arctic Oscillation signature in the wintertime geopotential height and temperature fields. *Geophys. Res. Lett.,* **25,** 1297–1300.

——, and ——, 2000: Annular modes in the extratropical circulation. Part I: Month-to-month variability. *J. Climate,* **13,** 1000–1016.

Thorncroft, C. D., and K. Hodges, 2001: African easterly wave variability and its relationship to Atlantic tropical cyclone activity. *J. Climate,* **14,** 1166–1179.

——, N. M. J. Hall, and G. N. Kiladis, 2008: Three-dimensional structure and dynamics of African easterly waves. Part III: Genesis. *J. Atmos. Sci.,* **65,** 3596–3607.

Trenberth, K. E., D. P. Stepaniak, and J. M. Caron, 2000: The global monsoon as seen through the divergent atmospheric circulation. *J. Climate,* **13,** 3969–3993.

Ventrice, M. J., C. D. Thorncroft, and M. A. Janiga, 2011: Atlantic tropical cyclogenesis: A three-way interaction between an African easterly wave, diurnally varying convection, and a convectively coupled atmospheric Kelvin wave. *Mon. Wea. Rev.,* **140,** 1108–1124.

Vera, C., and Coauthors, 2006: Toward a unified view of the American monsoon systems. *J. Climate,* **19,** 4977–5000.

Waliser, D. E., 2006: Intraseasonal variability. *The Asian Monsoon,* B. Wang, Ed., Springer, 203–258.

——, and M. Moncrieff, 2008: Year of Tropical Convection (YOTC): The YOTC Science Plan. WCRP–WWRP/THORPEX International Initiative WMO/TD-1452, 26 pp.

——, Z. Zhang, K.-M. Lau, and J.-H. Kim, 2001: Interannual sea surface temperature variability and the predictability of tropical intraseasonal variability. *J. Atmos. Sci.,* **58,** 2595–2614.

Wallace, J. M., 2000: North Atlantic Oscillation/annular mode: Two paradigms—one phenomenon. *Quart. J. Roy. Meteor. Soc.,* **126,** 791–805.

——, and D. S. Gutzler, 1981: Teleconnections in the geopotential height field during the Northern Hemisphere winter. *Mon. Wea. Rev.,* **109,** 784–812.

Wang, B., Ed., 2006: *The Asian Monsoon*. Springer, 844 pp.

Wang, C. Z., S.-K. Lee, and D. B. Enfield, 2008: Atlantic warm pool acting as a link between Atlantic multidecadal oscillation and Atlantic tropical cyclone activity. *Geochem. Geophys. Geosyst.,* **9,** Q05V03, doi:10.1029/2007GC001809.

Wang, H. L., and G. Feingold, 2009: Modeling mesoscale cellular structures and drizzle in marine stratocumulus. Part I: Impact of drizzle on the formation and evolution of open cells. *J. Atmos. Sci.,* **66,** 3237–3256.

Ward, M. N., 1998: Diagnosis and short-lead time prediction of summer rainfall in tropical North Africa at interannual and multidecadal timescales. *J. Climate,* **11,** 3167–3191.

Weickmann, K. M., G. R. Lussky, and J. E. Kutzbach, 1985: Intraseasonal (30–60 day) fluctuations of outgoing longwave radiation and 250 mb streamfunction during northern winter. *Mon. Wea. Rev.,* **113,** 941–961.

Wheeler, M., and G. N. Kiladis, 1999: Convectively coupled equatorial waves: Analysis of clouds and temperature in the wavenumber–frequency domain. *J. Atmos. Sci.,* **56,** 374–399.

——, and K. M. Weickmann, 2001: Real-time monitoring and prediction of modes of coherent synoptic to intraseasonal tropical variability. *Mon. Wea. Rev.,* **129,** 2677–2694.

——, and H. H. Hendon, 2004: An all-season real-time multivariate MJO index: Development of an index for monitoring and prediction. *Mon. Wea. Rev.,* **132,** 1917–1932.

Wood, R., K. K. Comstock, C. S. Bretherton, C. Cornish, J. Tomlinson, D. R. Collins, and C. Fairall, 2008: Open cellular structure in marine stratocumulus sheets. *J. Geophys. Res.,* **113,** D12207, doi:10.1029/2007JD009371.

——, C. S. Bretherton, D. Leon, A. D. Clarke, P. Zuidema, G. Allen, and H. Coe, 2010a: An aircraft case study of the spatial transition from closed to open mesoscale cellular convection over the southeast Pacific. *Atmos. Chem. Phys. Discuss.,* **10,** 17 911–17 980.

——, and Coauthors, 2010b: The VAMOS Ocean-Cloud-Atmosphere-Land Study Regional Experiment (VOCALS-REx): Goals, platforms, and field operations. *Atmos. Chem. Phys. Discuss.,* **10,** 20 769–20 822.

Zhang, C. D., 2005: Madden-Julian oscillation. *Rev. Geophys.,* **43,** RG2003, doi:10.1029/2004RG0001a58.

Zhou, J. Y., and K.-M. Lau, 1998: Does a monsoon climate exist over South America? *J. Climate,* **11,** 1020–1040.

Zhu, Y., and R. E. Newell, 1994: Atmospheric rivers and bombs. *Geophys. Res. Lett.,* **21,** 1999–2002.

——, and ——, 1998: A proposed algorithm for moisture fluxes from atmospheric rivers. *Mon. Wea. Rev.,* **126,** 725–735.